used as well for the *P. falciparum* counterpart PfCHT1 (short form having a catalytic domain only) to allow for direct enzymatic comparison [7].

2. Materials and methods

2.1. Plasmid constructs

The *P. vivax* PvCHT1 expression construct was prepared by PCR-amplifying the native coding sequence from *P. vivax* SalI genomic DNA excluding N-terminal signal peptide and repeat/insert region of *pvcht1* (GenBank accession no. AB106896) (Fig. 1A). The XhoI-containing 5′ primer was GAG ACT CGA GAT GGG AGG TAG CCA TGA TAG AAA ACC TCC (the restriction site underlined, and a start methionine codon typed in italic). The BamHI-containing 3′ primer was GAG AGG ATC CTC ACG CGT CTT CCT CTT GCT CAT AGG G. The deduced PvCHT1 protein begins at Gly-148 immediately downstream from the repeat/insert region, and terminated at Ala-648, the third residue upstream from the C terminus (501 residues). PCR products were restriction-digested, ligated in-frame into the XhoI and BamHI sites of the pEU-E01-HisGST(TEV) expression vector for wheat germ cell-free translation system, a slight modification from original pEU-E01-MCS (CellFree Sciences, Japan. http://www.cfsciences.com/eg/). This vector gives an N-terminal hexa-histidine and glutathione S-transferase (GST) tag followed by a tobacco etch virus (TEV) protease cleavage site upstream of cloned *pvcht1* (Fig. 1A). The construct was transfected into JM109 *E. coli* cells and the correct clone was verified by automated sequencing.

The second PvCHT1 expression construct was established by changing 3′ primer to GAG AGG ATC CTC ACC ATA CAT TCG TAA GGA ACG CAT CTA TAT, which gives shorter PvCHT1 terminating at Trp-494 (347 residues). This shorter construct mimicking such a short form chitinase as PfCHT1 covers only the common domain excluding putative chitin-binding domain (dotted on PvCHT1 in Fig. 1A).

The single copy gene *pfcht1* (accession no. AF172445) of *P. falciparum* chitinase (PfCHT1) was cloned into the same pEU-E01-HisGST(TEV) vector. This clone confers the identical PfCHT1 amino acid sequence, Gly-28 through His-378 (351 residues) to that used for previous study with conventional *E. coli* system [7] (Fig. 1A).

2.2. Recombinant protein synthesis by wheat germ cell-free system

We employed the wheat germ cell-free protein expression system for protein production using the bilayer translation reaction method described previously [13,17]. Briefly, 1.2 ml of transcription mixture containing 120 μg of the pEU vector construct, 80 mM HEPES-KOH, pH 7.8, 16 mM magnesium acetate, 2 mM spermidine, 10 mM dithiothreitol, 2.5 mM each of nucleotide triphosphates, 1 U/μl of SP6 RNA polymerase (Promega), and 1 U/μl of RNasin (Promega) was incubated 6 h at 37 °C. After the incubation, the solution with mRNA was centrifuged at 11,000 ×*g* for 5 min at 4 °C and supernatant was recovered and mixed with an equal volume (1.2 ml) of wheat germ extract (240 A_{260} units) (CellFree Sciences) supplemented with 2.4 μl of 20 mg/ml creatine kinase to prepare translation mixture. On top of 0.4 ml-each mixture aliquot in six-well plate, the 4.4 ml substrate mix containing 30 mM HEPES-KOH, pH 7.8, 100 mM potassium acetate, 2.7 mM magnesium acetate, 0.4 mM spermidine, 2.5 mM dithiothreitol, 0.3 mM each of 20 amino acids, 1.2 mM rATP, 0.25 mM rGTP, and 16 mM creatine phosphate were added and then incubated at 17 °C for 16 h.

2.3. Purification by affinity and anion-exchange chromatography

A 300 μl-bed volume of glutathione-coupled gel (Glutathione Sepharose 4B, GE Healthcare) was pre-equilibrated with 20 mM Tris–HCl (pH 8.0). The whole 28.8 ml of cell-free protein synthesis products was mixed with the gel and incubated for 16 h at 4 °C with gentle agitation. The suspension was then transferred into an empty column (Bio-Spin #732-6008, Bio-Rad Laboratories) and centrifuged at 500 ×*g* for 5 min. After washing the matrix pellet with 20 bed volumes (6 ml) of 20 mM Tris–HCl (pH 8.0), 3 and then 1 bed volume of elution buffer (10 mM reduced glutathione in the Tris-buffer above) were added to collect corresponding eluates E1 and E2.

Anion-exchange column chromatography was conducted on a 150 μl-bed volume of TOYOPEARL DEAE-650-M gel (TOSOH) in Bio-Spin column, pre-equilibrated with 20 mM Tris–HCl (pH 8.0). The E1 eluate above was added to the column and the gel matrix was washed primarily with 1.5 ml of 20 mM Tris–HCl (pH 8.0). The gel was next washed by 0.1 M and then 0.18 M sodium chloride in the same buffer, 0.3 ml each, into the combined eluates EA1. Sodium chloride was concentrated further to 0.5 M (0.75 ml) to collect EA2 eluate.

2.4. AcTEV protease treatment to remove His-GST portion

The 2.5 times EA2 concentrate (0.3 ml) by ultrafiltration (Ultrafree™ #UFV5BGC, 10 kDa molecular mass cutoff, Millipore) was mixed with 10 mU/μl (final) of AcTEV protease (Invitrogen) and incubated for 3 h at 30 °C. 0.2 ml of the product was further mixed with two different matrices, 9 μl of Glutathione Sepharose 4B and 3 μl of nickel-charged resin (Ni-NTA Superflow, Qiagen), pre-equilibrated with 20 mM Tris–HCl (pH 8.0). The mixture was incubated overnight at 4 °C and the supernatant including cleaved PvCHT1 molecules was separated by 0.22 μm microfiltration unit (Ultrafree™ #UFC30GV, Millipore) from His-GST portion on matrices. The solution was dialyzed overnight at 4 °C in the buffer containing 40 mM Tris–HCl, pH 7.5, 400 mM sodium chloride, 2 mM EDTA, and 0.2% TritonX-100. These recombinant PvCHT1 (rPvCHT1) or rPfCHT1 protein samples were finally mixed with an equal volume of 100% glycerol, either for immediate use or for storage at −25 °C until further use.

2.5. Immunization of mice and rabbit with rPvCHT1 and Pvs25

The purified rPvCHT1 proteins were suspended in 1× phosphate buffered saline (PBS). Groups of female BALB/c mice were subcutaneously immunized three times on days 0, 21, and 42 with 10 μg of the rPvCHT1 emulsified in Freund's adjuvant (complete for priming, incomplete Freund's adjuvant for subsequent immunizations). Antiserum was prepared as described elsewhere [18]. For obtaining polyclonal serum for counterstaining, the recombinant ookinete surface protein Pvs25 was administered subcutaneously (250 μg, 3 times) into a Japanese White rabbit following the same protocol [19].

2.6. Indirect immunofluorescence assay (IFA)

Blood specimens from gametocytemic *vivax* malaria patients were used as a source of zygotes/ookinetes produced *in vitro* [20]. The use of all human materials in this study was reviewed and approved by institutional Ethics committee of the Thai Ministry of Public Health and the Human Subjects Research Review Board of the United States Army. Peripheral blood was collected with heparinized syringes with written informed consent from patients who came to the malaria clinics in Mae Sod, Thailand. Infection with *P. vivax* was confirmed by microscopic observation of Giemsa-stained thick and thin blood smears.

Indirect immunofluorescence assays (IFAs) were performed with *P. vivax* zygotes/ookinetes acetone-fixed onto glass slides. After blocking in phosphate-buffered saline (PBS) containing 5% nonfat skim milk, the specimens were incubated 1 h at 37 °C with two primary antibodies in the same buffer, mouse anti-PvCHT1 antiserum (1:50 dilution) and rabbit anti-Pvs25 (1:200). After washing with 1× PBS, slides were then incubated 30 min at 37 °C with Alexa 488-labeled goat anti mouse IgG (1:500 dilution; Invitrogen), Alexa 546-labeled goat anti rabbit IgG (1:500; Invitrogen), and 4,6-diamidino-2-phenyl-indole HCl (DAPI, 1 μg/ml; Wako Pure Chemical). The slides were mounted with Prolong

Gold® (Invitrogen) and examined with LSM5 Pascal confocal laser microscope system (Carl Zeiss MicroImaging).

2.7. Assessment of chitinase activity

Chitinase activity of purified rPvCHT1 or rPfCHT1 aliquots was assayed by microfluorimetry using 4-methylumbelliferone (4MU) derivatives of chitin oligosaccharides (β-1,4-poly-*N*-acetyl glucosamine (GlcNAc)). The reaction volume of 200 μl in 96-well black round bottom plates (Corning) includes 0.1 mM Tris–HCl (pH 8.0), 1 mM sodium chloride, 5 μM EDTA, 0.005% (w/v) Triton X-100, and 19 μM of 4-methylumbelliferyl-*N,N′,N″*-β-D-triacetyl chitotrioside (4MU-$GlcNAc_3$) (Sigma-Aldrich). The production of 4MU during continuous incubation at 26 °C was monitored (Wallac ARVO™ MX 1420 multilabel counter (Perkin Elmer); excitation at 355 nm; emission at 450 nm). The resultant enzymatic activity was reported as initial rates of substrate hydrolysis per minute using a standard curve to transform relative fluorescent units. Quantification of proteins was done using Advanced Protein Assay™ reagent #ADV101 (Cytoskeleton).

2.8. Determination of substrate specificity, pH profile, temperature profile, and allosamidin inhibition curves

To assess substrate specificity of the recombinant *Plasmodium* chitinases, mono-, di-, and tri-GlcNAc derivatives of 4-methylumbelliferone (4MU-$GlcNAc_{1-3}$) (Sigma-Aldrich) were used in enzyme assays under the same conditions as described in Section 2.7. Only 4MU-$GlcNAc_3$ was used for the other three sets of test below. The pH activity profile was monitored at 26 °C using a potassium phosphate buffer (40 mM final with respect to phosphate) system, instead of Tris–HCl, with pH at 4.3 and ranging from 4.5 to 8.0 in 0.5 pH unit increments. The temperature activity profile was tested from 10 to 50 °C in 5 °C increments using standard Tris–HCl (pH 8.0) buffer. An inhibitor against family-18 chitinases, allosamidin (courtesy of Dr. Shohei Sakuda, University of Tokyo, Japan), was prepared as a 4 mM stock in 0.1 M acetate that was diluted just before assay into the standard reaction mixture in the previous section to estimate IC_{50} at fixed 19 μM 4MU-$GlcNAc_3$. The stock allosamidin solution was concentrated so that the solvent acetate did not cause pH fluctuation among working solutions at various allosamidin concentrations (data not shown). These experiments were repeated three times each.

3. Results and discussion

Recombinant protein of a chitinase from *P. vivax* (rPvCHT1) was successfully produced using the wheat germ cell-free translation system (Fig. 1A). rPvCHT1 shared general characteristics with the other *Plasmodium* family-18 chitinases, yet enzymatic characters varied in some details compared to *P. falciparum* recombinant PfCHT1 (rPfCHT1), as described below.

3.1. Enzymatically active PvCHT1 recombinant (r) protein, covering both catalytic and chitin-binding domains, was obtained using the wheat germ cell-free system (Fig. 1B)

A series of rPvCHT1 purification steps produced a prominent protein band with apparent mass of ~80 kDa in the eluate E1 after glutathione (GSH)/glutathione S-transferase (GST) affinity purification, which remained ~80 kDa after anion-exchange chromatography in the eluate EA2, and finally changed to ~60 kDa after AcTEV protease treatment (arrows in Fig. 1B). Another major band with less intensity was at 26–27 kDa in the E1 and separated into EA1 eluate (closed triangle) from the dominant band shown above. This profile is also the case with rPfCHT1; the dominant at 60–65 kDa in the E1 going down to ~40 kDa after AcTEV treatment, while the other band into EA1 at an identical 26–27 kDa indicating a contaminant GSH-binding protein from the wheat germ extract. The profile fits predicted molecular masses: full-length products of 85 kDa (rPvCHT1) or 57 kDa (rPfCHT1) from the constructs in the pEU-E01-HisGST(TEV) should be AcTEV-digested into common 28 kDa N-terminal His-GST portion (open triangle in Fig. 1B) and chitinase part with different sizes (arrows). Using the full long form of rPvCHT1, the chitinase-specific activities digesting 4-methylumbelliferyl-*N,N′,N″*-β-D-triacetyl chitotrioside (4MU-$GlcNAc_3$) were detected compared to mock reactions using protein synthesis products without template mRNA. The rPfCHT1 hydrolyzed 4MU-$GlcNAc_3$ as well, whereas the second (shortened) PvCHT1 construct lacking the putative chitin-binding domain did not show any hydrolyzing activity (data not shown). These results demonstrate for the first time that *P. vivax pvcht1* chitinase can be expressed successfully as an active recombinant protein, and that a putative chitin-binding domain which the *P. falciparum* paralog PfCHT1 lacks at its C-terminus is important for rPvCHT1 to exhibit its enzymatic activity.

Further confirmation of the activity of rPvCHT1 was demonstrated by assays during sequential purification steps. rPvCHT1 chitinase-specific activity increased with purity, but that of rPfCHT1 protein prepared in parallel was >100 times higher than rPvCHT1 at corresponding purification steps. This comparatively weak activity by rPvCHT1 on an artificial substrate 4MU-$GlcNAc_3$ led us to the other test for substrate specificity described in Section 3.3.

3.2. PvCHT1 was localized in cytoplasmic organelle of zygote/ookinete (Fig. 2)

To demonstrate the presence of PvCHT1 in *P. vivax* mosquito midgut stage parasites, immuno-localization assay was carried out. Confocal immunofluorescence microscopy with anti-rPvCHT1 on

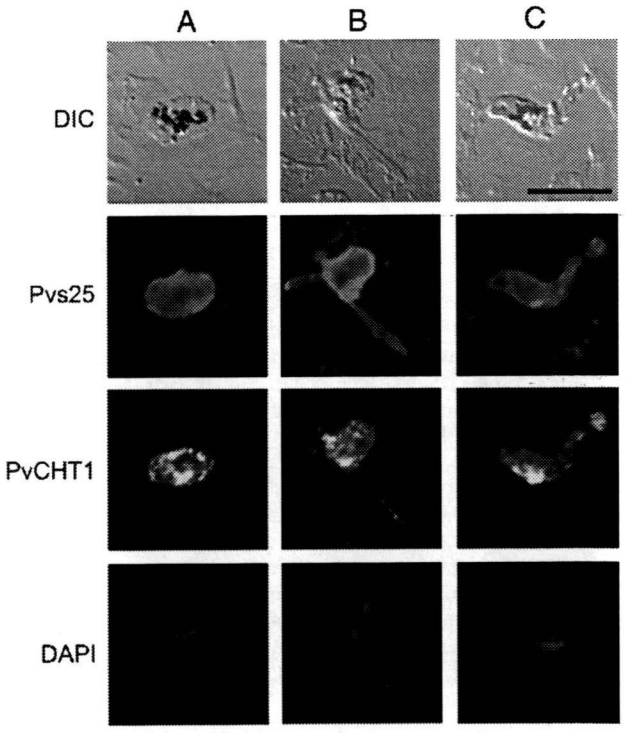

Fig. 2. Immunofluorescence localization of *P. vivax* chitinase PvCHT1 in *in vitro*-developed mosquito midgut stage parasites. Column A (left), zygote; B, immature ookinete; C, mature ookinete. Each of 3 columns consists of 4 panels showing from top to bottom; differential interference contrast (DIC) image, staining with rabbit anti-Pvs25 antiserum (red), with mouse anti-PvCHT1 (green), and DAPI-stained nuclei (blue). Bar = 10 μm. See Section 2.6. (For interpretation of the references to color in this figure legend, the reader is referred to the web version of this article.)

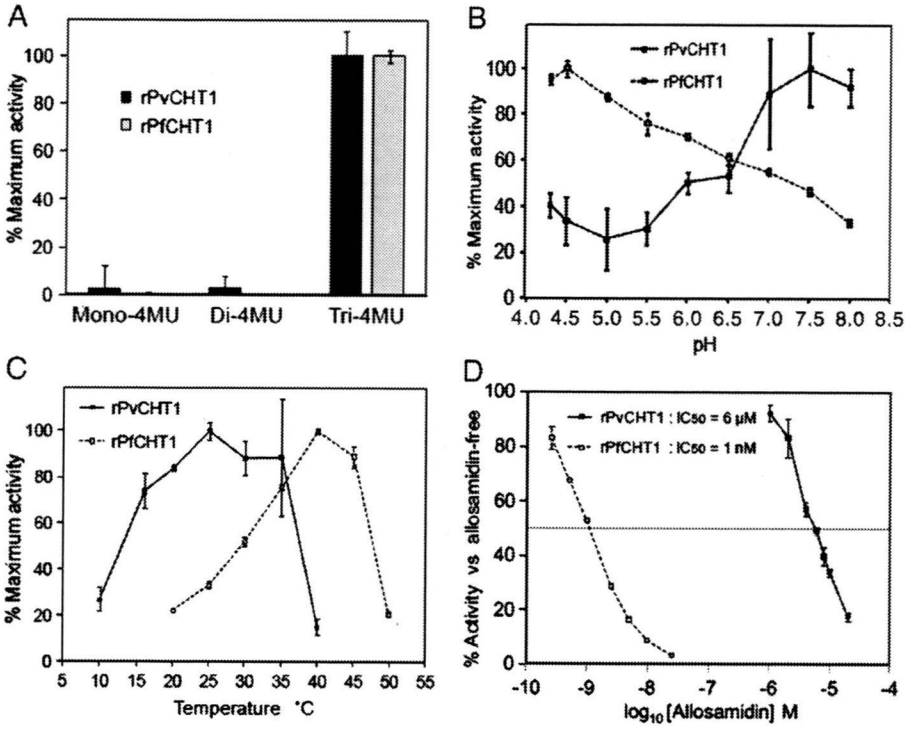

Fig. 3. Detailed analyses of chitinase activities by rPvCHT1 and rPfCHT1. Data with standard errors are displayed as the mean of three separate experiments. See Section 2.8. A. The substrate specificity. Quantification of fluorescence at 26 °C/pH 8.0 on 3 substrates with different number of *N*-acetyl-D-glucosamine (GlcNAc), 4MU-$GlcNAc_{1-3}$. Results are shown as relative rates of activities. B and C. pH or temperature activity profiles. Relative rates of activities at different (B) pH (at a constant temperature of 26 °C) or (C) temperature (at pH 8.0) levels. D. Allosamidin sensitivity on 4MU-$GlcNAc_3$ at 26 °C/pH 8.0. Chitinase activity is expressed as percent activity of enzyme in the absence of allosamidin.

P. vivax zygote/ookinetes demonstrated a nondiffuse, lumpy-granular, and uneven staining (green) throughout the different developmental stages. The PvCHT1 distributed in zygote cytoplasm as granular pattern (Fig. 2, column A), while in immature ookinetes, it was concentrated into zygote remnant space out of which the ookinete is emerging (B). In mature ookinetes there was the patchy appearance of the immunofluorescent signals of PvCHT1 mainly in anterior cytoplasm (C), suggesting the micronemal localization of PvCHT1. This localization was distinct from parasite surface membranes, as delineated by red staining of zygote/ookinete surface antigen Pvs25. The localization pattern of PvCHT1 is consistent with previous IFA studies on *P. gallinaceum* and *P. falciparum* [21] as well as that on *P. vivax* ookinete using anti-*P. gallinaceum* CHT1 active-site antiserum [11], indicating that recombinant PvCHT1 protein with the same immunological properties was successfully prepared.

3.3. The enzymatic characteristics of rPvCHT1, unlike rPfCHT1, were close to plasmodial long form chitinase PgCHT1 (Fig. 3)

We found that rPvCHT1 hydrolyses only 4MU-$GlcNAc_3$ but not 4MU-$GlcNAc_{1-2}$ (Fig. 3A). This substrate preference is shared not only with the rPfCHT1 prepared here with the wheat-germ cell-free system, but is also consistent with previous reports using *E. coli*-produced recombinant PfCHT1 [7] and recombinant PgCHT1 [8]; the same was observed with *P. gallinaceum* native chitinase activity by ookinete crude extracts [8]. These data indicate that PvCHT1 maintains the specificity unique to *Plasmodium* chitinases; an endochitinase with a preference for longer chitin oligosaccharides substrates.

We examined the rPvCHT1 pH activity profile, which demonstrated that optimal activity occurs under neutral condition (pH at 7.0–8.0 in Fig. 3B). It is unique among plasmodial chitinases examined so far, and is consistent with the pH 8.0–9.5 in the adult Anopheles mosquito midgut [22] and further with the pH 7.5–7.6 after bloodmeal ingestion [23]. As a control, rPfCHT1 produced in the wheat germ system was most active at pH 4.5, consistent with previous reports (optimal pH at 4.0–5.0) using native or recombinant proteins PfCHT1, PgCHT1 and PgCHT2 [7,8]. Although the physiological implications in this preference for lower pH by control rPfCHT1 is not instantly clear, it should be noted that the chitinase activity of rPfCHT1 at pH 8.0 still maintains >30% of its maximum at pH 4.5, suggesting that these Pf or Pg chitinases do as well work in the adult mosquitoes midgut. Furthermore, studies on chitinases from microbial sources including bacteria and fungi (Table 1 in review article [24] and references therein) suggest that the difference in optimum pH to this extent is not quite exceptional. The temperature activity profile examined here for the first time even for rPfCHT1 as well as rPvCHT1 (Fig. 3C) showed a preference of rPvCHT1 for relatively lower temperature (maximum at 25 °C and >80% max. at 20–35 °C) than rPfCHT1 (max. at 40 °C). The result is consistent with geographical prevalence of falciparum/vivax malaria; the former is in tropical region and the latter prefers more temperate environment. And it should be noted again that the studies on chitinases from microbial sources (Table 1 in [24]; the optimum Tm ranging from 30 to 60 °C) suggest that the results here by rPvCHT1 and rPfCHT1 are not quite exceptional.

rPvCHT1 was >1,000-fold less sensitive (IC_{50} = 6 µM) to the chitinase inhibitor allosamidin than rPfCHT1 (1 nM), when measured at a fixed concentration of substrate 4MU-$GlcNAc_3$ (19 µM) (Fig. 3D). If *Plasmodium* chitinases are grouped following the *P. gallinaceum* nomenclature into a long form (PgCHT1) and a short form (PgCHT2 lacking a putative chitin-binding domain), this difference was observed previously; the IC_{50} values were 12 µM and 7 µM respectively for recombinant and native PgCHT1 preparation, while as low as 0.3 µM for native PgCHT2 [8]. *P. falciparum* recombinant PfCHT1 produced in *E. coli* showed IC_{50} values around 0.1 µM (40–

150 nM) under different pH conditions of 5.0, 6.0 and 7.0 [7], a sensitivity much closer to its apparent ortholog PgCHT2 than to its paralog PgCHT1. The sensitivity of rPfCHT1 here produced by the wheat germ cell-free system ($IC_{50} = 1$ nM) is even more remarkable, whereas the IC_{50} (6 μM) of rPvCHT1 here is closer to its ortholog PgCHT1. However, it should also be noted that the 1 mM and 0.1 mM concentrations of allosamidin used in previous study to block oocyst development [4] far exceed this value, and they would completely inhibit *P. vivax* chitinase activity *in vivo*.

Collectively, these data in this first report of the functional property of the *P. vivax* chitinase, PvCHT1, indicate that it has most characteristics of *Plasmodium* chitinases. However more in enzymatic detail it is close to long forms represented by *P. gallinaceum* PgCHT1. Also taken into account the difference in the catalytic domain sequence between PvCHT1 and PfCHT1 (Introduction and Fig. 1A), it has yet to be determined whether a single strategy targeting both chitinases is feasible for human malaria transmission-blocking.

Acknowledgements

The authors are grateful for vivax malaria patients at Mae Sod district, Tak Province, Thailand for providing blood specimens, as well as the staff of the Vector Borne Disease Training Center, Pra Budhabat, Saraburi, Thailand, for assistance in setting up the field sites and the staff of the Department of Entomology, AFRIMS, Bangkok, Thailand. A chitinase specific inhibitor allosamidin is a kind gift from Dr. Shohei Sakuda, University of Tokyo, Japan. This work was supported in part by Grants-in-Aid for Scientific Research (17790277, 18390129 and 19406009) and Scientific Research on Priority Areas (19041053) from the Ministry of Education, Culture, Sports, Science and Technology of Japan, and grants from the U.S. National Institutes of Health (JMV).

References

[1] Huber M, Cabib E, Miller LH. Malaria parasite chitinase and penetration of the mosquito peritrophic membrane. Proc Natl Acad Sci U S A 1991;88:2807–10.
[2] Tsai YL, Hayward RE, Langer RC, Fidock DA, Vinetz JM. Disruption of *Plasmodium falciparum* chitinase markedly impairs parasite invasion of mosquito midgut. Infect Immun 2001;69:4048–54.
[3] Dessens JT, Mendoza J, Claudianos C, Vinetz JM, Khater E, Hassard S, et al. Knockout of the rodent malaria parasite chitinase pbCHT1 reduces infectivity to mosquitoes. Infect Immun 2001;69:4041–7.
[4] Shahabuddin M, Toyoshima T, Aikawa M, Kaslow DC. Transmission-blocking activity of a chitinase inhibitor and activation of malarial parasite chitinase by mosquito protease. Proc Natl Acad Sci U S A 1993;90:4266–70.
[5] Langer RC, Li F, Popov V, Kurosky A, Vinetz JM. Monoclonal antibody against the *Plasmodium falciparum* chitinase, PfCHT1, recognizes a malaria transmission-blocking epitope in *Plasmodium gallinaceum* ookinetes unrelated to the chitinase PgCHT1. Infect Immun 2002;70:1581–90.
[6] Li F, Templeton TJ, Popov V, Comer JE, Tsuboi T, Torii M, et al. *Plasmodium* ookinete-secreted proteins secreted through a common micronemal pathway are targets of blocking malaria transmission. J Biol Chem 2004;279:26635–44.
[7] Vinetz JM, Dave SK, Specht CA, Brameld KA, Xu B, Hayward R, et al. The chitinase PfCHT1 from the human malaria parasite *Plasmodium falciparum* lacks proenzyme and chitin-binding domains and displays unique substrate preferences. Proc Natl Acad Sci U S A 1999;96:14061–6.
[8] Vinetz JM, Valenzuela JG, Specht CA, Aravind L, Langer RC, Ribeiro JM, et al. Chitinases of the avian malaria parasite *Plasmodium gallinaceum*, a class of enzymes necessary for parasite invasion of the mosquito midgut. J Biol Chem 2000;275:10331–41.
[9] Langer RC, Li F, Vinetz JM. Identification of novel *Plasmodium gallinaceum* zygote- and ookinete-expressed proteins as targets for blocking malaria transmission. Infect Immun 2002;70:102–6.
[10] Li F, Patra KP, Vinetz JM. An anti-Chitinase malaria transmission-blocking single-chain antibody as an effector molecule for creating a *Plasmodium falciparum*-refractory mosquito. J Infect Dis 2005;192:878–87.
[11] Tsuboi T, Kaneko O, Eitoku C, Suwanabun N, Sattabongkot J, Vinetz JM, et al. Gene structure and ookinete expression of the chitinase genes of *Plasmodium vivax* and *Plasmodium yoelii*. Mol Biochem Parasitol 2003;130:51–4.
[12] Carlton JM, Adams JH, Silva JC, Bidwell SL, Lorenzi H, Caler E, et al. Comparative genomics of the neglected human malaria parasite *Plasmodium vivax*. Nature 2008;455:757–63.
[13] Sawasaki T, Ogasawara T, Morishita R, Endo Y. A cell-free protein synthesis system for high-throughput proteomics. Proc Natl Acad Sci U S A 2002;99:14652–7.
[14] Madin K, Sawasaki T, Ogasawara T, Endo Y. A highly efficient and robust cell-free protein synthesis system prepared from wheat embryos: plants apparently contain a suicide system directed at ribosomes. Proc Natl Acad Sci U S A 2000;97:559–64.
[15] Tsuboi T, Takeo S, Iriko H, Jin L, Tsuchimochi M, Matsuda S, et al. Wheat germ cell-free system-based production of malaria proteins for discovery of novel vaccine candidates. Infect Immun 2008;76:1702–8.
[16] Mudeppa DG, Pang CK, Tsuboi T, Endo Y, Buckner FS, Varani G, et al. Cell-free production of functional *Plasmodium falciparum* dihydrofolate reductase-thymidylate synthase. Mol Biochem Parasitol 2007;151:216–9.
[17] Sawasaki T, Hasegawa Y, Tsuchimochi M, Kamura N, Ogasawara T, Kuroita T, et al. A bilayer cell-free protein synthesis system for high-throughput screening of gene products. FEBS Lett 2002;514:102–5.
[18] Arakawa T, Komesu A, Otsuki H, Sattabongkot J, Udomsangpetch R, Matsumoto Y, et al. Nasal immunization with a malaria transmission-blocking vaccine candidate, Pfs25, induces complete protective immunity in mice against field isolates of *Plasmodium falciparum*. Infect Immun 2005;73:7375–80.
[19] Sattabongkot J, Tsuboi T, Hisaeda H, Tachibana M, Suwanabun N, Rungruang T, et al. Blocking of transmission to mosquitoes by antibody to *Plasmodium vivax* malaria vaccine candidates Pvs25 and Pvs28 despite antigenic polymorphism in field isolates. Am J Trop Med Hyg 2003;69:536–41.
[20] Suwanabun N, Sattabongkot J, Tsuboi T, Torii M, Maneechai N, Rachapaew N, et al. Development of a method for the in vitro production of *Plasmodium vivax* ookinetes. J Parasitol 2001;87:928–30.
[21] Langer RC, Hayward RE, Tsuboi T, Tachibana M, Torii M, Vinetz JM. Micronemal transport of *Plasmodium* ookinete chitinases to the electron-dense area of the apical complex for extracellular secretion. Infect Immun 2000;68:6461–5.
[22] del Pilar Corena M, VanEkeris L, Salazar MI, Bowers D, Fiedler MM, Silverman D, et al. Carbonic anhydrase in the adult mosquito midgut. J Exp Biol 2005;208:3263–73.
[23] Billker O, Miller AJ, Sinden RE. Determination of mosquito bloodmeal pH in situ by ion-selective microelectrode measurement: implications for the regulation of malarial gametogenesis. Parasitology 2000;120(Pt 6):547–51.
[24] Dahiya N, Tewari R, Hoondal GS. Biotechnological aspects of chitinolytic enzymes: a review. Appl Microbiol Biotechnol 2006;71:773–82.

Single amino acid substitution in *Plasmodium yoelii* erythrocyte ligand determines its localization and controls parasite virulence

Hitoshi Otsuki[a], Osamu Kaneko[a,b,1], Amporn Thongkukiatkul[a,c], Mayumi Tachibana[a], Hideyuki Iriko[a,d], Satoru Takeo[e], Takafumi Tsuboi[e], and Motomi Torii[a]

[a]Department of Molecular Parasitology, Ehime University Graduate School of Medicine, Toon, Ehime 791-0295, Japan; [b]Department of Protozoology, Institute of Tropical Medicine (NEKKEN) and the Global Center of Excellence Program, Nagasaki University, Nagasaki, Nagasaki 852-8523, Japan; [c]Department of Biology, Burapha University, Amphur Muang, Chonburi 20131, Thailand; [d]Department of Microbiology and Pathology, Faculty of Medicine, Tottori University, Yonago, Tottori 683-8503, Japan; and [e]Cell-Free Science and Technology Research Center, Ehime University, Matsuyama, Ehime 790-8577, Japan

Edited by Thomas E. Wellems, National Institutes of Health, Bethesda, MD, and approved February 23, 2009 (received for review November 10, 2008)

The major virulence determinant of the rodent malaria parasite, *Plasmodium yoelii*, has remained unresolved since the discovery of the lethal line in the 1970s. Because virulence in this parasite correlates with the ability to invade different types of erythrocytes, we evaluated the potential role of the parasite erythrocyte binding ligand, *Py*EBL. We found 1 amino acid substitution in a domain responsible for intracellular trafficking between the lethal and nonlethal parasite lines and, furthermore, that the intracellular localization of *Py*EBL was distinct between these lines. Genetic modification showed that this substitution was responsible not only for *Py*EBL localization but also the erythrocyte-type invasion preference of the parasite and subsequently its virulence in mice. This previously unrecognized mechanism for altering an invasion phenotype indicates that subtle alterations of a malaria parasite ligand can dramatically affect host–pathogen interactions and malaria virulence.

dense granule | invasion | malaria | microneme | transfection

The rodent malaria parasite *Plasmodium yoelii yoelii* has been widely studied to understand the interactions between the malaria parasite and the host cell (1). The nonlethal 17X line mainly infects young erythrocytes (reticulocytes), whereas the lethal 17XL and YM lines infect a wide range of erythrocytes. These lines have previously been studied to identify the genetic determinants of virulence (2, 3). These differences in erythrocyte invasion preference suggest the possible involvement of a parasite ligand that recognizes erythrocyte surface receptors; however, the actual molecular basis of the observed invasion preference differences remains unclear.

Erythrocyte invasion by the malaria merozoite is a multistep process, initiated by reversible binding to the erythrocyte surface, followed by the establishment of a tight junction between the apical end of the merozoite and erythrocyte surface and the subsequent movement of the merozoite into the nascent parasitophorous vacuole. Each step involves specific interactions between parasite ligands and erythrocyte receptors. Among the ligands of malaria parasites, the best characterized is a type I integral transmembrane protein encoded by the *ebl* (*erythrocyte-binding-like*) gene family. Upon release from the micronemes, EBL proteins recognize erythrocyte receptors and initiate the formation of the tight junction. The importance of EBL in malaria virulence is exemplified in the human malaria parasite *Plasmodium vivax*, which uses an EBL orthologue, *Pv*DBP, to recognize the Duffy antigen on the erythrocyte surface. Because the parasite is apparently unable to use an alternative invasion pathway, individuals in whom the Duffy antigen is not expressed on the erythrocyte surface are completely resistant to *P. vivax* (4, 5). Because of this dramatic association between the disruption of a host–pathogen interaction and protection against a malaria parasite, *Pv*DBP and the *Plasmodium falciparum* EBL orthologue, EBA-175, have been targeted for vaccine development (6).

EBL proteins possess 2 Cys-rich regions conserved among EBL orthologues. The N-terminal Cys-rich region named the DBL (Duffy-binding-like) domain or region 2 (7) recognizes a specific erythrocyte surface receptor. The C-terminal Cys-rich region named the C-cys domain or region 6 is located adjacent to the transmembrane domain, and the number and location of Cys residues are well conserved among known *Plasmodium* species. Region 6 exhibits structural similarity to the KIX-binding domain of the coactivator CREB-binding protein (8) and has been proposed to be a protein trafficking signal for transportation to the micronemes (9). Here we report a single nonsynonymous nucleotide substitution in the *pyebl* gene between lethal and nonlethal lines of *P. yoelii* and show the effect of this substitution on the intracellular localization of EBL, erythrocyte-type preference, and consequently virulence of *P. yoelii*.

Results

To investigate differences in EBL between lethal and nonlethal *P. yoelii* lines, we compared sequences from a variety of malaria parasite species and *P. yoelii* lines 17X, 17XL, and YM. We found 1 nonsynonymous nucleotide substitution in region 6 between the nonlethal 17X and lethal 17XL lines in the entire ORF (Fig. 1). The nonlethal 17X line possesses 8 conserved Cys residues that form 4 disulfide bridges (8), whereas the lethal 17XL line possesses an Arg instead of Cys at the second Cys position. This substitution was also found in another lethal line, "YM" (2), which originated independently from the 17X line during serial passage (3). All *Plasmodium* EBL orthologues for which protein expression was validated possess 8 conserved Cys residues in this region, further indicating that these Cys residues play an important role (supporting information Fig. S1). Thus the observed substitution from Cys to Arg is likely to abolish the native conformation of region 6.

EBL Localizes in the Dense Granules in *P. yoelii* Line 17XL. We raised specific polyclonal and monoclonal antibodies against *Py*EBL

Author contributions: H.O., O.K., and M. Torii designed research; H.O., A.T., M. Tachibana, H.I., and S.T. performed research; T.T. contributed new reagents/analytic tools; H.O., O.K., and M. Torii analyzed data; and H.O. and O.K. wrote the paper.

The authors declare no conflict of interest.

This article is a PNAS Direct Submission.

Data deposition: The data reported in this article have been deposited in the GenBank/European Molecular Biology Laboratory/DNA Data Base in Japan databases (accession nos. AB430781–AB430789).

[1]To whom correspondence should be addressed. E-mail: okaneko@nagasaki-u.ac.jp.

This article contains supporting information online at www.pnas.org/cgi/content/full/0811313106/DCSupplemental.

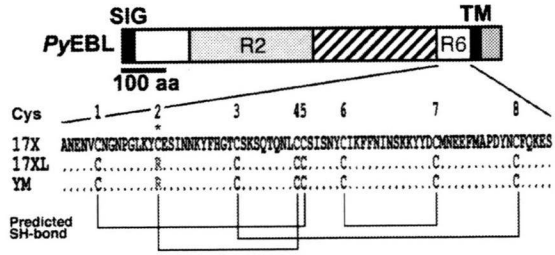

Fig. 1. Schematic structure of *P. yoelii* EBL (*Py*EBL). SIG, TM, R2, and R6 indicate the putative endoplasmic reticulum transporting signal, the transmembrane region, region 2, and region 6, respectively. Amino acid alignment of *Py*EBL from 17X, 17XL, and YM lines are shown below. Eight conserved Cys residues that form disulfide bridges (Predicted SH-bond) and the substitution from Cys to Arg (*) are indicated.

and performed Western blot analysis. The *Py*EBL protein was detected as a 110-kDa band in both the 17X and 17XL lines (Fig. 2*A*). The intracellular localization of *Py*EBL in both the 17X and 17XL lines was compared by indirect immunofluorescent assay

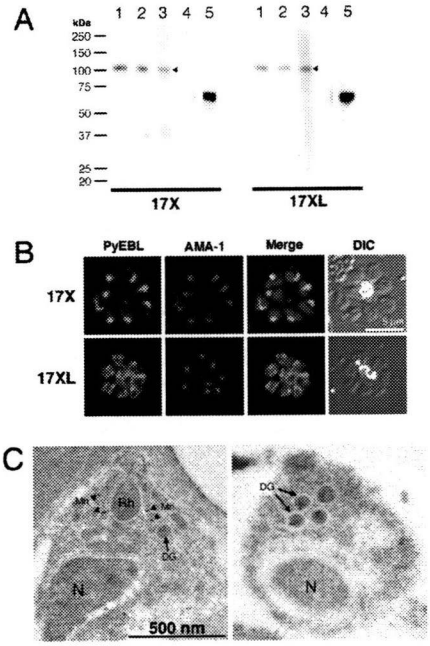

Fig. 2. Western blot analysis and *Py*EBL localization in *P. yoelii* schizont by immunostaining. (*A*) Western blot analysis with mAb 5B10 (lane 1), mAb 1G10 (lanes 2), and mouse serum (lane 3) specific for *Py*EBL against purified *P. yoelii* schizont extracts. A 110-kDa band was detected in both 17X and 17XL lines, with no significant difference in the protein expression level (arrowheads). This band was not detected by normal mouse serum (lane 4). Anti-AMA1 serum detected a 66-kDa band at similar levels (lane 5). (*B*) *P. yoelii* schizonts were incubated with mAb 5B10 (PyEBL), rabbit anti-AMA1 serum (AMA1), and DAPI (blue) for nuclear staining. Schizonts labeled with anti-*Py*EBL (5B10) were stained with FITC secondary antibody (green). Anti-AMA1 were stained with Alexa-546 secondary antibody (red). DIC images are shown in the right-hand column. The 17X line shows apical *Py*EBL signal colocalized with AMA1, but the region 6–substituted 17XL line shows diffused staining that does not colocalize with AMA1. (*C*) Immunoelectron microcopy was carried out for resin-embedded *P. yoelii* 17X and 17XL lines with anti-*Py*EBL mouse serum and secondary antibody conjugated with gold particles. *Py*EBL was detected in the micronemes (arrowheads) of the 17X line, but in the 17XL line it was located in the dense granules (arrows). N, nucleus; Mn, microneme; DG, dense granule; Rh, rhoptry.

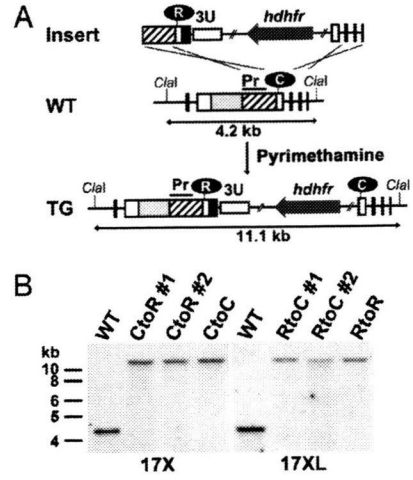

Fig. 3. Amino acid replacement of *Py*EBL region 6 second cysteine location by targeted recombination. (*A*) Schematic representation of the WT and modified (TG) *pyebl* gene loci. The replacement cassette (Insert) was inserted into the *pyebl* gene locus by double-crossover recombination. In this schematic, the second Cys in region 6 was replaced with Arg in the 17X line to generate 17X-CtoR. Other transgenic lines were generated in a similar fashion. ClaI restriction sites and the expected size of the DNA fragment after ClaI digestion are shown. Pr, probe region used in Southern blot analysis. (*B*) Southern blot analysis of the *pyebl* gene locus in WT and transgenic parasite lines derived from *P. yoelii* 17X and 17XL. The absence of the 4.2-kb WT band and the presence of an 11.1-kb band indicate that the *Py*EBL locus was modified in all transgenic clones.

(IFA) using specific antibodies against *Py*EBL (Fig. S2). In the 17X line, *Py*EBL localized to the apical end of each merozoite in both the segmented schizont-stage parasite and individual merozoites, where it colocalized with AMA1, a known microneme protein, under immunofluorescent microscopy (Fig. 2*B*). However, in the 17XL line *Py*EBL did not colocalize with AMA1 at the apical end of merozoites and showed a more diffused but granular distribution in comparison with parasites of the 17X line (Fig. 2*B*). Diffused localization of *Py*EBL was also observed in parasites of the YM line (Fig. S3). Immunoelectron microscopy revealed that *Py*EBL localized in micronemes in the 17X line as reported for *P. falciparum* and *Plasmodium knowlesi* (10, 11). In the 17XL line, however, *Py*EBL localized not in the microneme but in another microorganelle—the dense granules (12) (Fig. 2*C* and Fig. S4).

Because there seems to be only 1 copy of *Py*EBL in the genomes of both lines (Fig. S5), and significant differences were not observed in the level of transcription and protein expression between the 17X and 17XL lines (Fig. 2*A* and Fig. S6), the location of EBL seems to be the most significant difference between them.

Genetic Replacement of Arg and Cys in Region 6 Alters EBL Localization. To evaluate whether the Arg substitution at the second Cys position is responsible for the altered trafficking of *Py*EBL, we exchanged Cys and Arg in the 17X and 17XL lines by genetic modification (17X-CtoR and 17XL-RtoC). The parasites were also transfected with control constructs that do not alter the region 6 amino acid sequence (17X-CtoC and 17XL-RtoR) (Fig. 3*A*). Each of the transgenic parasites was evaluated for the correct integration of the constructs to the *pyebl* gene locus by specific PCR analysis followed by sequencing of the PCR-amplified products (not shown) and Southern blot analysis (Fig. 3*B*).

In the 17X line, replacement of Cys with Arg (17X-CtoR) altered the *Py*EBL localization from an apical pattern to a

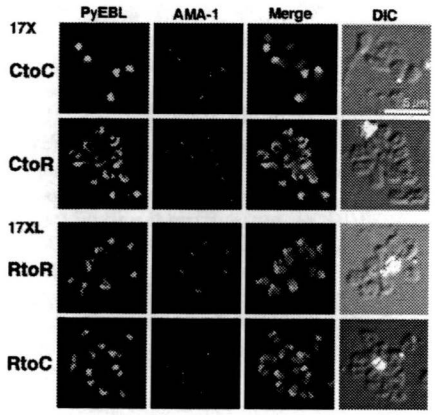

Fig. 4. Replacement of Cys to Arg in region 6 altered subcellular localization of *Py*EBL. Schizonts of transgenic parasite lines were incubated with mAb 5B10 (PyEBL), rabbit anti-AMA1 serum (AMA1), and DAPI (blue) for nuclear staining. DIC images are shown in the right-hand column. In the 17X background, control (CtoC) shows an apical *Py*EBL signal colocalized with AMA1, but replaced (CtoR) shows a 17XL pattern. Inversely, 17XL background control (RtoR) shows a diffused nonapical pattern, but replaced to cysteine (RtoC) shows an apical signal colocalized with AMA1.

nonapical diffused pattern, and *Py*EBL did not colocalize with AMA1. Furthermore, the replacement of Arg with Cys in the 17XL line (17XL-RtoC) altered the *Py*EBL localization from a nonapical diffused pattern to an apical pattern. Control parasites did not display altered *Py*EBL localization (Fig. 4). These results confirm that the observed substitution from Cys to Arg is responsible for the altered localization of *Py*EBL from micronemes to dense granules in the 17XL line.

EBL Localization Alters Erythrocyte-Type Preference and Course of Infection. To determine whether altered localization of *Py*EBL affects erythrocyte-type invasion preference, infected erythrocytes were examined by microscopy, and a selectivity index (SI) was obtained by calculating multiple parasite infection of single erythrocytes for each parasite line on postinfection day 3 in mice (13). We found that 17XL-RtoC predominantly invaded reticulocytes in the same way as the nonlethal 17X line. The SI of the 17XL line (2.38) was increased in 17XL-RtoC (≈35; $P < 0.001$). On the other hand, 17X-CtoR was able to invade a variety of ages of erythrocytes, including mature erythrocytes, comparable to the lethal 17XL line, with the SI of the 17X line (16.78) reduced in 17X-CtoR (≈4; $P < 0.001$; Table 1). These results demonstrate that the localization of *Py*EBL is responsible for the erythrocyte-type preference of the parasite.

Table 1. Selectivity index of WT and transgenic *Plasmodium yoelii* lines

Parasite	*n*	Selectivity index (range)
17X-CtoR 1	5	3.87 (1.86–5.32)
17X-CtoR 2	5	4.25 (2.38–7.97)
17X-CtoC	5	23.53 (16.49–36.00)
17X	5	16.78 (7.60–24.99)
17XL-RtoC 1	5	34.35 (29.18–38.05)
17XL-RtoC 2	5	35.99 (29.97–42.72)
17XL-RtoR	5	1.31 (0.57–2.13)
17XL	5	2.38 (1.58–3.75)

Selectivity indices were calculated from parasitized Giemsa-stained thin blood films collected from each infection.

Because erythrocyte-type preference frequently correlates with virulence in malaria parasites, we further analyzed the transgenic *P. yoelii* parasites for differences in the course of infection and survival of parasite-infected mice. Mice infected with the 17XL-RtoC line developed significantly lower parasitemias compared with the parental 17XL and control 17XL-RtoR lines (Fig. 5*A*), with 100% survival (Fig. 5*C*), whereas all mice infected with 17XL and 17XL-RtoR lines died by day 7 (Fig. 5*C*). The pattern observed for the 17XL-RtoC line was identical to that observed for the nonlethal 17X line. Thus, trafficking of *Py*EBL to the micronemes causes the virulence of the 17XL line to be reduced to the same level as the nonlethal 17X line, suggesting that *Py*EBL is a critical virulence determinant in the 17XL line. The parasitemia of mice infected with 17X-CtoR increased significantly compared with those infected with parental 17X and control 17X-CtoC lines during the acute phase of infection on days 4 to 5 ($P < 0.001$). However, the parasitemia did not reach the level observed for the lethal 17XL line, and it reduced to the same level observed for the 17X and 17X-CtoC lines by day 9 (Fig. 5*B*). No parasites were detectable by microscopy at day 17 (not shown). This suggests that the 17X-CtoR line is able to invade a greater repertoire of erythrocyte types than 17X but is unable to invade as many types as the 17XL line. This reduced capacity to invade multiple erythrocyte types compared with the 17XL line results in a nonlethal infection, in which all mice survive (Fig. 5*C*). Thus, displacement of the EBL from microneme was not sufficient to make this line fully lethal, suggesting the existence of other determinant(s).

Discussion

The results of this study indicate that replacement of Cys to Arg at the second Cys position of *Py*EBL region 6 is the major

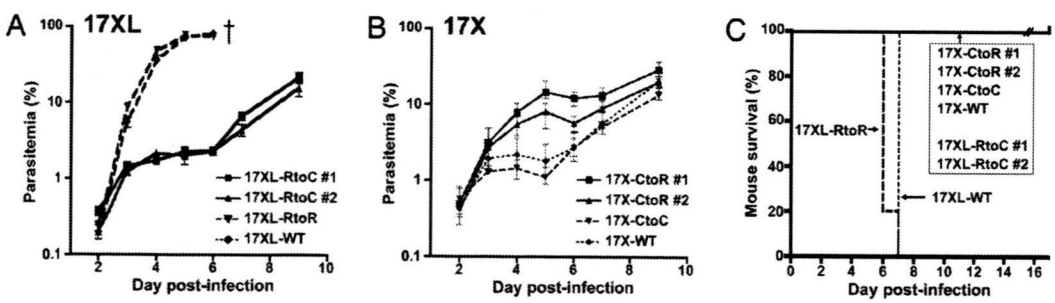

Fig. 5. Effect of the alteration of *pyebl* gene loci on the course of infection and parasite virulence in mice. Mice were i.v. inoculated with 1×10^6 parasitized erythrocytes from WT or transgenic parasite lines. (*A*) Parasitemia of 17XL-RtoC was dramatically reduced to the same level as that of the nonlethal 17X line. (*B*) Parasitemia of 17X-CtoR was significantly higher than parental 17X and control 17X-CtoC on days 4 and 5 ($P < 0.001$), the acute phase of infection; however, the pattern observed is intermediate between the lethal 17XL and nonlethal 17X lines. Parasitemias are plotted using the geometric mean and SD of log-transformed data from groups of 5 mice. (*C*) All mice infected with 17XL-RtoC survived, whereas all mice infected with parental 17XL and control 17XL-RtoR lines died by day 7. All mice infected with 17X, 17X-CtoC, and 17X-CtoR survived.

determinant of the difference between lethal and nonlethal lines of *P. y. yoelii* parasites. This substitution alters the intracellular organelle localization of *Py*EBL from the micronemes to the dense granules and alters the erythrocyte-type invasion preference, course of infection, and parasite virulence in the host.

The crystal structure of region 6 of *P. falciparum* EBA-175 indicates that the second Cys residue forms a disulfide bridge with the fourth Cys residue in this region. Arg substitution of the second Cys residue in the *P. yoelii* 17XL line abolishes this disulfide bridge and thus likely destroys the region 6 structure, which is critical for the trafficking of the protein to the micronemes. It is possible that an incorrectly folded region 6 would not allow the protein to be properly recognized by an (as yet uncharacterized) partner molecule responsible for the trafficking of the EBL protein to the micronemes (9). The mechanism involved in the trafficking of the mutated protein to the dense granules remains unresolved.

Using genetic modification, we have demonstrated that when *Py*EBL is trafficked to the microneme in the 17XL line genetic background, the erythrocyte-type invasion preference and the course of infection are comparable to those of the nonlethal 17X line. This indicates that the substitution of Cys to Arg is a major determinant of the lethal phenotype of the 17XL line. However, when *Py*EBL was not trafficked to the microneme in parasites with the 17X line genetic background, the course of infection was intermediate between the 2 parental lines, suggesting that although *Py*EBL is a critical determinant, other factor(s) are also involved in the lethal phenotype of the 17XL line. In *P. falciparum*, the expression of EBL seems to be co-operationally regulated with another *Plasmodium* ligand encoded by the *rbl (reticulocyte-binding-like)* multigene family that is composed of 6 members in *P. falciparum* and at least 14 members in *P. yoelii* (14–16); thus, the *P. yoelii rbl* protein, Py235, is a potential candidate for such factor(s). Consistent with this hypothesis is the finding that when Py235 expression was suppressed, the course of infection of the lethal *P. yoelii* YM line was altered from a lethal pattern to an intermediate pattern similar to that observed in the 17X-CtoR line shown in this study (17). On the basis of these observations, we propose that *Py*EBL may preferentially recognize reticulocytes and that the removal of *Py*EBL from the micronemes may result in free space within this organelle that may subsequently be filled with other ligand(s), possibly Py235, which consequently enables the parasite to invade a variety of erythrocyte types. Because different Py235 proteins may have different receptor specificities, parasite invasion preference and the subsequent course of infection may vary, depending on the Py235 member that fills the free space in the micronemes created by the absence of *Py*EBL. Such a switching mechanism for an erythrocyte invasion pathway has been previously proposed for *P. falciparum* (18).

A Linkage Group Selection analysis conducted by Pattaradilokrat et al. (19) identified a chromosomal region that included the *ebl* gene locus as a major determinant in the multiplication rate differences between the lethal *P. y. yoelii* YM line and a nonlethal 33X line, supporting the role of the EBL protein in controlling virulence phenotypes. Consistent with our findings that another genetic factor may be involved, they also identified a further genomic region on *P. yoelii* chromosome 5 or 6 that showed weak association with multiplication rate.

Because *Py*EBL localized in the dense granules is potentially nonfunctional, we attempted to disrupt the *pyebl* gene locus in both the 17X and 17XL lines (Fig. S7). However, repeated attempts failed to achieve this, despite the successful genomic integration of the control plasmid. This indicates that *Py*EBL is essential for parasite survival, even when it is not trafficked to the microneme. Two possible explanations for this may be that (*i*) an undetectable amount of *Py*EBL may still localize in the micronemes and remain functional, or (*ii*) *Py*EBL is functional during erythrocyte invasion (or for another unknown critical role during the life cycle), even when localized in the dense granules. Although a subgroup of the dense granules, known as exonemes, were recently reported to secrete their contents immediately before schizont rupture (20), we found that *Py*EBL was not detected on the surface of released individual merozoites of 17XL parasites (Fig. S8). Thus, the identity of the *Py*EBL-containing dense granules and the timing of *Py*EBL secretion from them, if at all, in the 17XL line remain undetermined.

In summary, we have found that a single nucleotide substitution altered the intracellular localization of the malaria parasite ligand *Py*EBL, which in turn altered erythrocyte invasion preference, course of infection, and parasite virulence. The virulence-mediating mechanism described in this report furthers our understanding of parasite–host interactions and has important implications for malaria vaccine design, especially those based on *Pv*DBP for *P. vivax* malaria.

Materials and Methods

Rodent Malaria Parasites. *Plasmodium yoelii* 17X, 17XL, and YM lines were maintained in BALB/c mice (Charles River Japan). The *P. yoelii* YM line was a kind gift from David Walliker of Edinburgh University.

DNA and RNA Isolation. Parasite genomic DNA (gDNA) was isolated from parasite-infected mouse blood using DNAzol BD reagent (Invitrogen). Parasite-infected blood was passed through a single CF11 cellulose column to remove leukocytes, and a schizont-enriched fraction was collected by differential centrifugation on a 50% Percoll solution (GE Healthcare). Total RNA was isolated from the schizont-enriched fraction using RNeasy Mini Kit (Qiagen). cDNA was synthesized using Omniscript reverse transcriptase (Qiagen) with random hexamer after DNase treatment.

PCR Amplification and Sequencing of *ebl* Genes. *ebl* genes were PCR-amplified from gDNA using KOD Plus DNA polymerase (Toyobo), with specific primers for each *ebl* gene designed using the *P. yoelii* genome database (The Institute for Genomic Research) and the *P. chabaudi* and *P. berghei* genome databases (The Sanger Centre). *ebl* sequences were determined by direct sequencing using an ABI PRISM 310 genetic analyzer (Applied Biosystems) from PCR-amplified products. Sequences were aligned using CLUSTALW implemented in MacVector (version 9.0; Accelrys).

Southern Blot Analysis. Five micrograms of *P. yoelii* gDNA were digested with EcoRI, EcoRV, ClaI, BanI, and NspI, and with BanI and HpaI with appropriate buffer, overnight. Digested gDNA was subjected to electrophoresis on 0.8% agarose gels, followed by alkaline transfer onto a Hybond-*n* + PVDF membrane (GE Healthcare). Probes were first PCR-amplified with 5′–TAAATCTAAATGGGATACAT–3′ and 5′–AGTTGGATTGATAGTTACAGATTC–3′ primers for the *pyebl* region, cloned into pGEM-T Easy plasmid (Promega), digested from the plasmid, and then hybridized onto membranes. Probes were labeled with the AlkPhos Direct kit (GE Healthcare), and a chemiluminescent signal developed with CDP-*star* reagent (GE Healthcare) was recorded on RX-U film (Fujifilm).

Recombinant Proteins. Expression plasmids were constructed on the basis of the pEU-E01-G(TEV)-N2 vector (21) by inserting PCR products amplified from *P. yoelii* 17X gDNA using KOD Plus DNA polymerase with the following primers: 5′-gagaCTCGAGGTTAATTTATTAAAAAGAACATATGAATCTTTCC-3′ and 5′-tctcGGATCC**CTA**TGAATAGCTCTCTTTTTGAAAAC-3′ for *Py*EBL regions 1 to 6 (R1–6; amino acid positions 28–787), 5′-gagaCTCGAGGTTAATTTATTAAAAAGAACATATGAATCTTTCC-3′ and 5′-tctcGGATCC**CTA**CAAATTATTATTAATAGGAGTATTACTGGG-3′ for regions 1 to 2 (R1–2; 28–436), 5′-gagaCTCGAGGAAAAAAATGGAAATGTAAATTACAAAG-3′ and 5′-tctcGGATCC**CTA**CAAATTATTATTAATAGGAGTATTACTGGG-3′ for region 2 (R2; 113–436), 5′-gagaCTCGAGTCTTCTGTTAAACCCAGTAATAC-3′ and 5′-tctcGGATCC**CTA**TACATTTTCGTTGGCTAGC-3′ for regions 3 to 5 (R3–5; 423–716), and 5′-gagagagaCTCGAGGACCCTAAACATGTATGTGTTGATAC-3′ and 5′-gagagagaGGATCC**TCA**TCCCATAAAGCTGGAAGAACTACAG-3′ for the 19-kDa region of the merozoite surface protein 1, *Py*MSP1 (*Py*MSP1–19; 1658–1757). The stop codon is shown in bold letters, and XhoI and BamHI restriction sites are underlined. GST-fused *Py*EBL or *Py*MSP1–19 recombinant proteins were expressed using the wheat germ cell-free protein synthesis system (Protemist DT; CellFree Sciences). Recombinant proteins were captured by a glutathione

column, washed, and eluted with glutathione elution buffer. Protein synthesis was confirmed by SDS-PAGE and Coomassie Brilliant Blue protein staining. Recombinant *Py*EBL R1–6 and R3–5 and *Py*MSP1–19 were used to produce antibodies, and *Py*EBL R1–2 and R2 were used for Western blot analysis.

Antibodies. To produce mouse anti-*Py*EBL and anti-*Py*MSP1 sera, female BALB/c mice were i.p. immunized 5 times with recombinant *Py*EBL R1–6 or 3 times with recombinant *Py*MSP1–19 emulsified with Freund's adjuvant, and killed for serum collection. To produce rabbit anti-*Py*EBL R3–5 serum, a female Japanese white rabbit was s.c. immunized 3 times with recombinant *Py*EBL R3–5 emulsified with Freund's adjuvant. To produce mouse anti-*Py*EBL monoclonal antibodies, the spleen was removed from a mouse immunized with recombinant *Py*EBL R1–6, and spleen cells were fused with a mouse myeloma cell line derived from a BALB/c mouse by the conventional polyethylene glycol method. Supernatants of cultured hybridoma colonies were tested with recombinant *Py*EBL R1–6 by ELISA and on *P. yoelii* 17X blood smears by indirect immunofluorescent assay. Positive hybridoma colonies were selected and cloned by 2 rounds of limiting dilution. The epitope region of each monoclonal antibody was tested by Western blot with a panel of recombinant *Py*EBL proteins. Anti-AMA1 rabbit serum was a gift from Carole Long of the National Institutes of Health.

Immunofluorescence Microscopy. *P. yoelii*–infected mouse erythrocytes were smeared onto glass slides, air dried, and stored at −80 °C without fixation. Slides were thawed, acetone-fixed, preincubated with PBS containing 5% nonfat milk at 37 °C for 30 min, incubated with mouse anti-*Py*EBL and rabbit anti-AMA1 sera at room temperature for 1 h, and then incubated with FITC-conjugated goat anti-(mouse IgG and IgM) antibody (Biosource International) and Alexa-546–conjugated goat antirabbit IgG antibody (Molecular Probes) at 37 °C for 30 min. Parasite nuclei were stained with DAPI. Differential interference contrast (DIC) and fluorescent images were obtained using a fluorescence microscope (BX50; Olympus) with a CCD digital camera (DC500; Leica) and processed using Adobe Photoshop CS (version 8.0; Adobe Systems).

Immunoelectron Microscopy. *P. yoelii*–infected mouse blood was fixed in 1% paraformaldehyde–0.1% glutaraldehyde in Hepes-buffered saline and embedded in LR white resin (Polysciences). Sections were blocked for 30 min in PBS–milk–Tween 20, incubated overnight at 4 °C in PBS–milk–Tween 20 containing mouse anti-*Py*EBL R1–6 serum, and then incubated for 1 h in PBS–milk–Tween 20 containing goat antimouse IgG conjugated with gold particles (10 nm diameter; Jansen). Sections were stained with 2% uranyl acetate in 50% methanol and examined by electron microscopy (JEM-1230; JEOL).

Genetic Modification of the *pyebl* Gene Locus. Two basic plasmids, pPbDT3U-B12 and pHDEF1-mh-R12, were constructed. A DNA fragment encoding cyan fluorescent protein was PCR-amplified from pECFP-C1 plasmid (Stratagene) using KOD Plus DNA polymerase with primers 5′-agcGCTAGCGTGAG-CAAGGGCGAG-3′ (NheI site is underlined) and 5′-gacGTCGAC**GGATCC**TCTA-GACTTGTACAGCTCGTCC-3′ (SalI and XbaI sites are underlined, and BamHI site is shown in bold) and ligated into the pGEM-T Easy plasmid. The insert was then digested with NheI and SalI, purified, and ligated into pRGDT-B12 (22) using the NheI and SalI sites, yielding pRCDT-B12. pRCDT-B12 was digested with ClaI and XbaI and filled with an oligonucleotide linker comprising cgatCTCGAG**CCCGGG**t and ctaga**CCCGGG**CTCGAGat to generate XhoI (underlined) and SmaI (bold) sites to yield pPbDT3U-B12. pHDEF1-mh (23) was digested with SmaI and ApaI to remove the 3′ untranslated region of histidine-rich protein 2, the ApaI cohesive end was blunted, and a Gateway gene conversion cassette C1 (Invitrogen) was inserted. The XhoI site was destroyed by XhoI digestion, filled in using KOD Plus DNA polymerase, and self-ligated to yield pHDEF1-mh-R12.

To modify the *pyebl* gene locus, a DNA fragment encoding *Py*EBL region 6 to the stop codon was PCR-amplified from gDNA of the *P. yoelii* 17XL line with primers 5′-gCCATGGGAACATAGAGACATTAAAAAAAGC-3′ and 5′-gCTCGAGATAAAAATCTACAGGTATATATTC-3′ (NcoI and XhoI sites are underlined) and cloned into pGEM-T Easy plasmids. The insert was ligated into the NcoI and XhoI sites of pPbDT3U-B12 to yield pR6Cyt-B12. DNA fragments encoding *Py*EBL region 3 to the stop codon were PCR-amplified from cDNA of the *P. yoelii* 17X and 17XL lines with primers 5′-atCTTCTGTTA-AACCCAGTAATAC-3′ and 5′-ccAGATCTTTAATAAAAATCTACAGG-TATATATTC-3′ (BglII site is underlined). PCR products were then ligated into the SmaI site of pR6Cyt-B12, yielding pR6Cyt+R3Cyt(X)-B12 and pR6Cyt+R3Cyt(XL)-B12, respectively. pR6Cyt+R3Cyt(X)-B12 and pR6Cyt+R3Cyt(XL)-B12 were subjected to a BP recombination reaction with the donor vector pDONR221 (Invitrogen) to produce the corresponding entry plasmids pENT.R6Cyt+R3Cyt(X) and pENT.R6Cyt+R3Cyt(XL). These entry plasmids were subjected to a LR recombination reaction (Invitrogen), according to the manufacturer's instructions, with pHDEF-1-mh-R12 to yield replacement constructs pYEBL-R6Cyt+R3Cyt(X) and pYEBL-R6Cyt+R3Cyt(XL), respectively.

P. yoelii schizont-enriched fraction was collected by differential centrifugation on 50% HistoDenz in PBS, and 20 μg of XhoI-digested transfection constructs were electroporated to 5×10^7 of enriched schizonts using the Nucleofector device (Amaxa) with human T cell solution under program U-33 (24). Transfected parasites were i.v. injected into 8-week-old BALB/c female mice, which were treated by i.p. injection with 1 mg/kg of pyrimethamine daily. Before inoculation of 17X line parasites, mice were treated with phenylhydrazine to increase the reticulocyte population in the blood. Drug-resistant parasites were cloned by limiting dilution. Integration of the transfection constructs was confirmed by PCR amplification with a unique set of primers for the modified *pyebl* gene locus, followed by sequencing and Southern blot analysis.

Course of Infection. To assess the course of infection of transgenic and WT parasite lines, 1×10^6 parasitized erythrocytes were injected i.v. into 8-week-old female BALB/c mice. Thin blood smears were made daily, stained with Giemsa's solution, and parasitemias were recorded. Mouse survival was evaluated by the Kaplan-Meier method. Parasitemias of each group were compared by 1-way ANOVA and Tukey's posttest, implemented in Prism 4.0 (GraphPad Software).

Selectivity Index. To compare erythrocyte preference between transgenic and WT *P. yoelii* parasite lines, a SI was calculated as follows: Multiple-infected erythrocytes divided by the expected number of multiple-infected erythrocytes, which was calculated from the number of infected erythrocytes and parasitemia (13). When the preferred erythrocyte type is limited, the observed number of multiple-infected erythrocytes increases. More than 200 parasitized erythrocytes were examined on Giemsa-stained thin blood smears collected on postinoculation day 3. The SI of each group was compared by 1-way ANOVA and Tukey's posttest, implemented in Prism 4.0.

For additional information see *SI Materials and Methods.*

ACKNOWLEDGMENTS. We thank D. Walliker for *P. yoelii* 33X, 33XPr3, and YM lines; C. Long for anti-AMA1 rabbit serum; H. A. del Portillo (Barcelona Centre for International Health Research, Barcelona) for pHDEF1-mh; Y. Tanaka, K. Kameda, and K. Oka (Integrated Center for Science, Ehime University) for their expertise; N. Kangwanrangsan (Ehime University, Matsuyama, Japan) for anti-*Py*MSP1–19 serum; and R. Culleton for critical reading. Preliminary sequence data for *P. berghei*, *P. chabaudi*, and *P. vinckei* were obtained from The Institute for Genomic Research. Animal experiments were carried out in compliance with the Guide for Animal Experimentation at Ehime University School of Medicine. This work was supported in part by Grants-in-Aids for Scientific Research 19790308 (to H.O.), 19590428 (to O.K.), 16390126 and 19390120 (to M. Torii), by Scientific Research on Priority Areas 19041053 (to T.T.) from the Ministry of Education, Culture, Sports, Science and Technology of Japan, and by Japan Society for the Promotion of Science–National University of Singapore Joint Research Program 07039011–000161 (to O.K.).

1. Landau I, Gautret P (1998), in *Malaria: Parasite Biology, Pathogenesis, and Protection*, ed Sherman IW (American Society for Microbiology, Washington, DC), pp 401–417.
2. Yoeli M, Hargreaves B, Carter R, Walliker D (1975) Sudden increase in virulence in a strain of *Plasmodium berghei yoelii*. *Ann Trop Med Parasitol* 69:173–178.
3. Playfair JH, De Souza JB, Cottrell BJ (1977) Protection of mice against malaria by a killed vaccine: Differences in effectiveness against *P. yoelii* and *P. berghei*. *Immunology* 33:507–515.
4. Miller LH, Mason SJ, Clyde DF, McGinniss MH (1976) The resistance factor to *Plasmodium vivax* in blacks. The Duffy-blood-group genotype, FyFy. *N Engl J Med* 295:302–304.
5. Wertheimer SP, Barnwell JW (1989) Plasmodium vivax interaction with the human Duffy blood group glycoprotein: Identification of a parasite receptor-like protein. *Exp Parasitol* 69:340–350.
6. Greenwood BM, et al. (2008) Malaria: Progress, perils, and prospects for eradication. *J Clin Invest* 118:1266–1276.
7. Adams JH, et al. (1992) A family of erythrocyte binding proteins of malaria parasites. *Proc Natl Acad Sci USA* 89:7085–7089.
8. Withers-Martinez C, et al. (2008) Malarial EBA-175 region VI crystallographic structure reveals a KIX-like binding interface. *J Mol Biol* 375:773–781.
9. Treeck M, et al. (2006) A conserved region in the EBL proteins is implicated in microneme targeting of the malaria parasite *Plasmodium falciparum*. *J Biol Chem* 281:31995–32003.

10. Sim BK, Toyoshima T, Haynes JD, Aikawa M (1992) Localization of the 175-kilodalton erythrocyte binding antigen in micronemes of *Plasmodium falciparum* merozoites. *Mol Biochem Parasitol* 51:157–159.
11. Adams JH, et al. (1990) The Duffy receptor family of *Plasmodium knowlesi* is located within the micronemes of invasive malaria merozoites. *Cell* 63:141–153.
12. Torii M, Adams JH, Miller LH, Aikawa M (1989) Release of merozoite dense granules during erythrocyte invasion by *Plasmodium knowlesi*. *Infect Immun* 57:3230–3233.
13. Simpson JA, Silamut K, Chotivanich K, Pukrittayakamee S, White NJ (1999) Red cell selectivity in malaria: A study of multiple-infected erythrocytes. *Trans R Soc Trop Med Hyg* 93:165–168.
14. Stubbs J, et al. (2005) Molecular mechanism for switching of *P. falciparum* invasion pathways into human erythrocytes. *Science* 309:1384–1387.
15. Iyer J, Grüner AC, Rénia L, Snounou G, Preiser PR (2007) Invasion of host cells by malaria parasites: A tale of two protein families. *Mol Microbiol* 65:231–249.
16. Carlton JM, et al. (2002) Genome sequence and comparative analysis of the model rodent malaria parasite *Plasmodium yoelii yoelii*. *Nature* 419:512–519.
17. Iyer JK, Amaladoss A, Ganesan S, Preiser PR (2007) Variable expression of the 235 kDa rhoptry protein of *Plasmodium yoelii* mediate host cell adaptation and immune evasion. *Mol Microbiol* 65:333–346.
18. Duraisingh MT, Maier AG, Triglia T, Cowman AF (2003) Erythrocyte-binding antigen 175 mediates invasion in *Plasmodium falciparum* utilizing sialic acid-dependent and -independent pathways. *Proc Natl Acad Sci USA* 100:4796–4801.
19. Pattaradilokrat S, Culleton RL, Cheesman SJ, Carter R (2009) Gene encoding erythrocyte binding ligand linked to blood stage multiplication rate phenotype in *Plasmodium yoelii yoelii*. *Proc Natl Acad Sci USA*, 10.1073/pnas.0811430106.
20. Yeoh S, et al. (2007) Subcellular discharge of a serine protease mediates release of invasive malaria parasites from host erythrocytes. *Cell* 131:1072–1083.
21. Tsuboi T, et al. (2008) Wheat germ cell-free system-based production of malaria proteins for discovery of novel vaccine candidates. *Infect Immun* 76:1702–1708.
22. Ghoneim A, Kaneko O, Tsuboi T, Torii M (2007) The *Plasmodium falciparum* RhopH2 promoter and first 24 amino acids are sufficient to target proteins to the rhoptries. *Parasitol Int* 56:31–43.
23. Fernandez-Becerra C, de Azevedo MF, Yamamoto MM, del Portillo HA (2003) Plasmodium falciparum: New vector with bi-directional promoter activity to stably express transgenes. *Exp Parasitol* 103:88–91.
24. Janse CJ, et al. (2006) High efficiency transfection of *Plasmodium berghei* facilitates novel selection procedures. *Mol Biochem Parasitol* 145:60–70.

Molecular & Biochemical Parasitology 170 (2010) 100–104

Contents lists available at ScienceDirect

Molecular & Biochemical Parasitology

Short communication

Characterization of two isotypes of L-threonine dehydratase from *Entamoeba histolytica*☆

Afzal Husain[a,b], Ghulam Jeelani[a,c], Dan Sato[c,d], Vahab Ali[b,1], Tomoyoshi Nozaki[a,*]

[a] Department of Parasitology, National Institute of Infectious Diseases, 1-23-1 Toyama, Shinjuku-ku, Tokyo 162-8640, Japan
[b] Department of Parasitology, Gunma University Graduate School of Medicine, Maebashi, Gunma 371-8511, Japan
[c] Center for Integrated Medical Research, School of Medicine, Keio University, Shinjuku, Tokyo 160-8582, Japan
[d] Institute for Advanced Biosciences, Keio University, Tsuruoka, Yamagata 997-0052, Japan

ARTICLE INFO

Article history:
Received 14 August 2009
Received in revised form 2 November 2009
Accepted 12 November 2009
Available online 18 November 2009

Keywords:
Amino acid
Metabolism
Serine
Threonine
Anaerobic protozoa

ABSTRACT

The genome sequence of the enteric protozoan parasite *Entamoeba histolytica* suggests that amino acid catabolism plays an important role in energy metabolism. In the present study, we described kinetic and regulatory properties of catabolic L-threonine and L-serine dehydratase (TD) from *E. histolytica*. TD catalyses the pyridoxal phosphate-dependent dehydrative deamination of L-threonine and L-serine to ammonia and keto acids (2-oxobutyrate and pyruvate, respectively). *E. histolytica* possesses two TD isotypes (EhTD1-2) showing 38% mutual identity, a calculated molecular mass of 45.0 or 46.5 kDa, and an isoelectric point of 6.68 or 5.88, respectively. Only EhTD1 showed L-threonine and L-serine dehydrative deaminating activities whereas EhTD2, in which the amino acid residues involved in the substrate and cofactor binding were not conserved, was devoid of these activities. The k_{cat}/K_m value of EhTD1 was >3 fold higher for L-threonine than L-serine. EhTD1 was inhibited by L-cysteine in a competitive manner with the K_i values of 1.1 mM and 2.2 mM for L-serine and L-threonine, respectively. EhTD1 was insensitive to the allosteric activation by AMP or CMP. Three major substitutions of EhTD1 likely attribute to the insensitivity. EhTD1 was also inhibited about 50% by 20 mM 2-oxobutyrate, pyruvate, and glyoxylate; the inhibition was not, however, reversed by AMP. Together, these data showed that EhTD1 possesses unique regulatory properties distinct from other organisms and may play an important role in energy metabolism via amino acid degradation in *E. histolytica*.

L-threonine dehydratase (TD, EC 4.3.1.19) belongs to the systematic subclass of ammonia lyases (EC 4.3.1), and catalyzes deamination of L-threonine to yield ammonia and 2-oxobutylate (Fig. 1A) via an intermediary dehydration [1]. The enzyme from a number of sources also acts on L-serine to yield pyruvate [1]. Most TDs have been shown to contain pyridoxal phosphate (PLP) as a prosthetic group, forming a Schiff base with the ε-amino moiety of a specific lysyl residue [2]. These dehydratases may serve catabolic or biosynthetic purposes and hence are ubiquitous. Biosynthetic TD catalyzes the first reaction in the isoleucine biosynthetic pathway. In all biosynthetic TDs studied so far, isoleucine or valine is the negative or positive allosteric effector, respectively [3]. Catabolic TD catalyzes the first reaction in the anaerobic breakdown of L-threonine to propionate [4]. Catabolic TD is insensitive to L-isoleucine and L-valine and activated by AMP [4].

E. histolytica, the causative agent of human amoebiasis, is an enteric protozoan parasite and causes amoebic colitis and extra intestinal abscesses [5]. *E. histolytica*, like other anaerobic or microaerophilic parasitic protozoa such as *Giardia lamblia* and *Trichomonas vaginalis*, lacks features of eukaryotic aerobic metabolism including the tricarboxylic acid (TCA) cycle and oxidative phosphorylation, and energy generation is primarily by substrate level phosphorylation [6]. Glycolysis under anaerobic conditions can use only part of the energy contained in glucose for ATP generation. The *E. histolytica* genome sequence suggests that ATP can be generated from amino acids [7]. This finding is further supported by the fact that *E. histolytica* trophozoites grown in axenic medium take up several amino acids when glucose is not available [8]. Amino acid degradation can produce either pyruvate or other 2-keto acids (Fig. 1A). Pyruvate:ferredoxin oxidoreductase (PFOR) is known to have a relaxed specificity. PFOR oxidatively decarboxylates pyru-

Abbreviations: TD, threonine dehydratase; EhTD, *Entamoeba histolytica* threonine dehydratase; PLP, pyridoxal 5′-phosphate; CMP, cytosine monophosphate; PCR, polymerase chain reaction.

☆ *Note:* The nucleotide sequence data of *Entamoeba histolytica* TD1 and TD2 reported in this paper are available at the DDBJ/GenBank®/EBI data bank with accession numbers AB511882 and AB511883.

* Corresponding author. Tel.: +81 3 5285 1111x2600; fax: +81 3 5285 1219.
E-mail address: nozaki@nih.go.jp (T. Nozaki).
[1] Present address: Department of Biochemistry, Rajendra Memorial Research Institute of Medical Sciences, Agamkuan, Patna 800007, India.

0166-6851/$ – see front matter © 2009 Elsevier B.V. All rights reserved.
doi:10.1016/j.molbiopara.2009.11.004

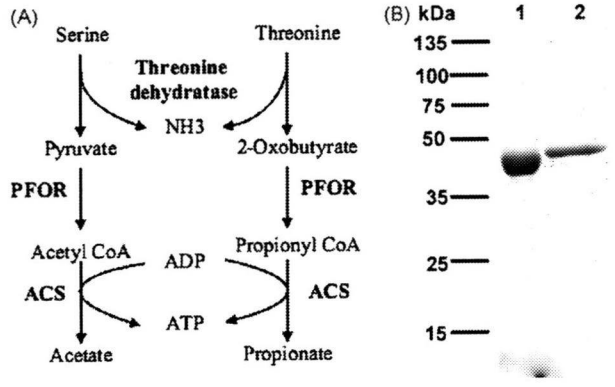

Fig. 1. (A) Presumed pathways of threonine and serine catabolism in *E. histolytica*. Abbreviations are: PFOR, pyruvate:ferredoxin oxidoreductase; ACS, acetyl CoA synthetase. (B) SDS-PAGE analysis of purified rEhTD1 and rEhTD2. Samples were electrophoresed on a 12.0% polyacrylamide gel and stained with Coomassie brilliant blue. Lanes 1 and 2 showed rEhTD1 and rEhTD2, respectively, eluted with 200 mM imidazole and dialyzed.

vate and 2-oxobutyrate to generate acetyl CoA and propionyl CoA, respectively [9]. Acetyl CoA synthetase (ACS), which is responsible for generating ATP via acetyl-CoA hydrolysis, also accepts propionyl-CoA as a substrate [10], completing the proposed pathway for ATP generation from various amino acids (Fig. 1A).

It was shown that L-serine and L-threonine are incorporated by *E. histolytica* trophozoites in the presence or absence of glucose [8]. It was also demonstrated that addition of L-serine to the culture medium stimulates oxygen consumption [11]. While the fate of L-serine and L-threonine after incorporation and the mechanisms of the augmented oxygen consumption by L-serine remain unknown, these facts indeed suggest the importance of serine metabolism in the *E. histolytica* energy production. In the present study, we have characterized for the first time, catabolic TD in trophozoites of an axenic HM-1:IMSS cl6 strain of *E. histolytica* [12].

We identified three genes encoding TD isotypes by homology search against the *E. histolytica* genome database [7] using TD protein sequences from bacteria, plants, and mammals. Since the third TD isotype (EHI_126080) is almost identical (98%) to the first TD (EHI_092390) with only a few amino acid changes at the amino and carboxyl termini of the protein, we did not further analyze the third TD. We accordingly designated the first and second putative TD genes as *EhTD1* and *EhTD2* [corresponding to EHI_092390 (AB511882) and EHI_049910 (AB511883)], respectively. Each of *EhTD1* and *EhTD2* genes contains a 1272-bp and 1290-bp open reading frame, which encodes the protein of 423 and 429 amino acid residues with a predicted molecular mass of 45.0 and 46.5 kDa, and p*I* of 6.68 and 5.88, respectively. The amino acid sequence of EhTDs showed 20–49% identities to TDs from archaea, bacteria, animals, and plants. EhTD1 and EhTD2 showed highest amino acid identities to TDs from an anaerobic thermohalophilic *Halothermothrix orenii* and a thermophilic uncultivable bacterium, dependent on microbial commensalism, *Symbiobacterium thermophilum* (49% and 38%, respectively). The identity between EhTD1 and EhTD2 was only 38%. Both EhTDs were devoid of the amino-terminal transit peptide, which suggests that amoebic TD genes encode cytosolic proteins.

A multiple alignment of EhTD isotypes with *Salmonella typhimurium* TD, by the Clustal W program (http://clustalw.ddbj.nig.ac.jp/top-e.html), showed that most of the important residues implicated in substrate and cofactor binding, as predicted from the crystal structure of *S. typhimurium* TD, were well conserved in EhTD1. However, there were a few substitutions of the amino acids for substrate binding: Tyr-153, Cys-238, and Ala-284 of *S. typhimurium* TD to Phe-169, Ile-254, and Ser-300 in EhTD1 [4], respectively (Fig. 2, "A"). In contrast, there were more substitutions in EhTD2 compared to EhTD1. In EhTD2, Pro-152, Tyr-153, Gln-162, Gly-237, and Cys-238 of *S. typhimurium* TD were substituted with Ala-175, Arg-176, Asp-185, Thr-260, and Asp-261, respectively ("B"). The tetraglycine loop, which is involved in the formation of hydrogen bonds with the phosphate moiety of PLP [4], was conserved in EhTD1, whereas the residues in the loop were partially altered in EhTD2 (Ser-208 and Ser-210, "C"). Among the amino acid residues involved in the binding of CMP and AMP, EhTD1 showed a few substitutions of Arg-53, Asp-119, and Gln-275 of *S. typhimurium* TD to Lys-69, Gly-135, and Glu-291 in EhTD1, respectively "D"). EhTD2 was devoid of the residues required for AMP and CMP binding, except for Tyr-143, Lys-301, and Asn-336, corresponding to Tyr-120, Lys-278, and Asn-314 of *S. typhimurium* TD (substituted residues are marked "E"). Phylogenetic analysis of EhTDs with TD protein sequences from various organisms did not clearly indicate the source of the amebic TD, but suggested that *E. histolytica* TDs were not obtained by lateral gene transfer (data not shown). EhTDs form a well-supported clade with catabolic TDs, but not with biosynthetic TDs from other organisms, which suggests the absence of biosynthetic TDs and isoleucine/valine biosynthetic pathway in *E. histolytica*.

To demonstrate enzymatic properties of the putative EhTD proteins, the recombinant EhTD1 and 2 were produced by prokaryotic expression system. The open reading frame of the individual TD genes was PCR amplified using *E. histolytica* cDNA library [13], platinum pfx DNA polymerase (Life Technologies, Tokyo, Japan), and oligonucleotide primers: 5′-cctCATATGacagagggaagtgaatactt-3′ and 5′-ccaGGATCCttacttgaaaacatatccagc-3′ (EhTD1); 5′-cctCATATGagtgacgtagaagttcctgca-3′ and 5′-ccaGGATCCttagacaaagacaaattcata-3′ (EhTD2), where capital letters indicate *Nde*I and *Bam*HI restriction sites. The PCR fragments were digested with *Nde*I and *Bam*HI, electrophoresed, purified with Geneclean kit II (BIO 101, Vista, CA, USA), and cloned into *Nde*I and *Bam*HI-double-digested pCold1 (Takara, Tokyo, Japan) to produce pCold1-EhTD1 and pCold1-EhTD2. *Escherichia coli* BL21 (DE3) cells (Takara) were transformed by one of these plasmids and grown in LB medium containing 50 μg/ml ampicillin with 1 mM of isopropyl β-D-thio galactopyranoside at 15 °C for 24 h. *E. coli* cells were harvested, washed with PBS, pH 7.4, lysed and centrifuged at 25,000 × *g* for 15 min at 4 °C. The supernatant containing N-terminal histidine-tagged EhTD1 or EhTD2 was purified with Ni^{2+}-NTA His-bind resin (Life Technologies). The purity of products was assessed to be >95% by SDS polyacrylamide gel electrophoresis stained with Coomassie brilliant blue (Fig. 1B).

TD activity was measured on the basis of the production of α-keto acids. The amount of α-keto acids generated was determined either colorimetrically [14] or spectrophotometrically at 310 nm [15]. Both rEhTD1 and rEhTD2 showed specific PLP peaks at 413 nm, suggesting the presence of PLP as a prosthetic group. The maximum activity of rEhTD1 was observed at slightly basic pH (8.5–9.0). The inclusion of 2 mM dithiothreitol in the reaction mixture enhanced enzymatic activity by >2 fold. EDTA at 1 mM also slightly enhanced activity. Unlike rEhTD1, rEhTD2 was devoid of putative serine dehydratase or TD activity under the conditions aforementioned. The lack of TD activity in EhTD2 may be attributable to the improper folding due to prokaryotic expression system or to the absence of the amino acid residues known to be involved in substrate and cofactor binding. We also examined whether 20 amino acids and 12 related compounds are degraded by rEhTD2, by incubating the mixture of potential substrates with rEhTD2, followed by measuring the concentrations of the substrates and their products by capillary electrophoresis-mass spectrometry [16]. However, we were unable to detect any degraded compounds (data not shown).

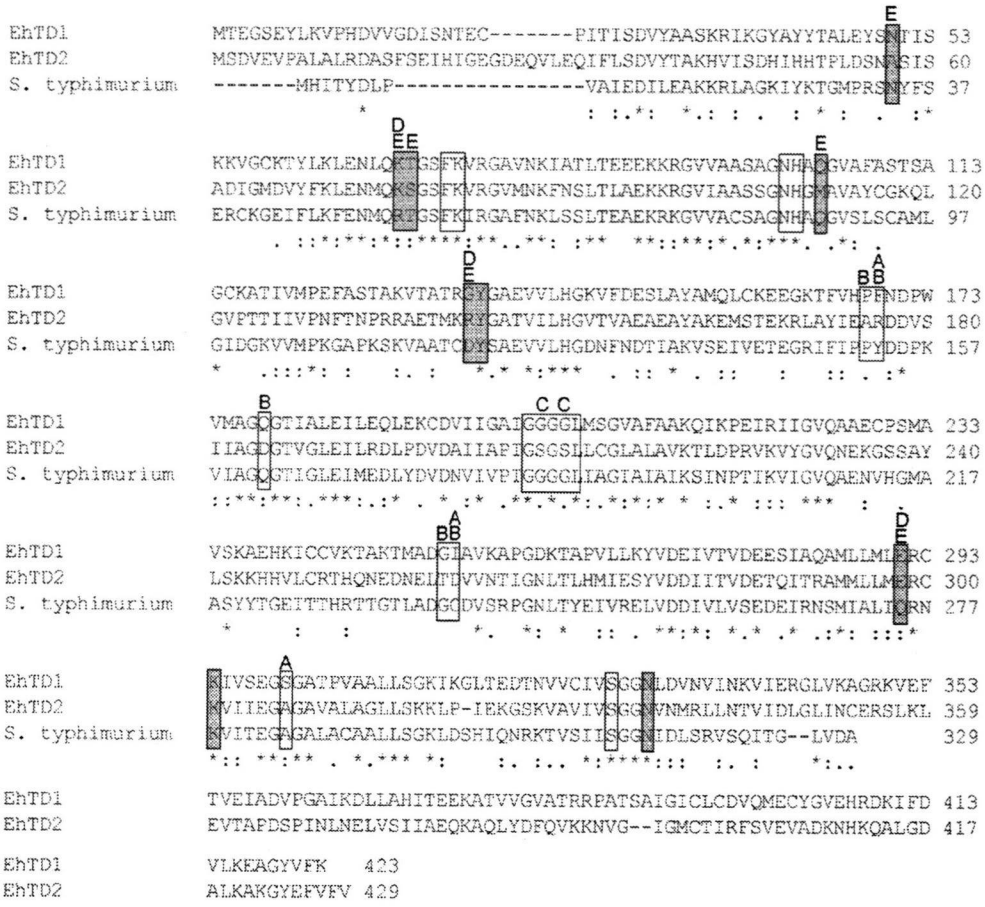

Fig. 2. Sequence alignment of threonine dehydratase from *E. histolytica* and *S. typhimurium*. Two *E. histolytica* (EhTD1 and EhTD2) and *S. typhimurium* (NP_462158) sequences were aligned using the CLUSTAL W program. Dashes indicate gaps. The highly conserved residues known to participate in the binding to substrates and PLP on the basis of crystal structures of *S. typhimurium* TD [4] are shown in open boxes, whereas the residues involved in AMP/CMP binding are shown in shaded boxes. Substituted amino acids in the substrate binding domains of EhTD1 and EhTD2 are depicted by "A" and "B", respectively, while those in the PLP binding domains of EhTD2 are depicted by "C". Substituted amino acids in the AMP/CMP binding domains of EhTD1 and EhTD2 are depicted by "D" and "E", respectively.

The K_m and k_{cat} values of rEhTD1 for L-serine and L-threonine were significantly different (Table 1). At saturating concentrations of substrates, rEhTD1 showed an approximately 2 fold higher affinity for L-threonine than L-serine. The k_{cat} of rEhTD1 was also 1.7-fold higher for L-threonine than L-serine. EhTD1 showed a ~3 fold higher k_{cat}/K_m value for L-threonine than L-serine, suggesting that EhTD1 primarily acts on L-threonine to generate 2-oxobutyrate, and also utilizes serine, at higher concentrations, to generate pyruvate. The premise that EhTD1 functions at relatively high L-serine concentrations was further supported by the previous study showing that serine supplementation to the culture medium caused increased oxygen consumption, most probably by increased synthesis of pyruvate [11]. The intracellular concentrations of L-serine and L-threonine under *in vitro* culture conditions are 3.2 and 4.5 mM, respectively [17]. Thus, EhTD1 preferentially degrades L-threonine, but not L-serine unless its kinetic properties are modulated by unknown factors and mechanisms *in vivo*. We also tested structurally related amino acids (L-homoserine, *O*-phospho-L-serine, *O*-acetyl-L-serine, *N*-acetyl-L-serine, *O*-succinyl-L-homoserine, and cystathionine) as substrates, but no activity was observed against these substrates.

The effect of L-cysteine and DL-homocysteine on the activity of rEhTD1 was examined. Like TDs from bacteria, animals, and plants [18], rEhTD1 was also inhibited by L-cysteine, but no significant inhibition was observed by DL-homocysteine up to 4 mM. Double reciprocal plots in the presence or absence of L-cysteine, showed that EhTD1 is inhibited by L-cysteine at physiological concentrations (K_i, 1.1 and 2.2 mM for L-serine and L-threonine, respectively), similar to the TDs from other organisms [19]. The inhibition by L-cysteine was more prominent when L-serine is used as a substrate

Table 1
Kinetic parameters of recombinant *E. histolytica* TD1.

Substrate	K_m (mM)	k_{cat} (s^{-1})	k_{cat}/K_m	K_i (mM) for L-cysteine	Mode of inhibition
L-serine	13.5 ± 0.8	3.0 ± 0.5	0.2 ± 0.1	1.1 ± 0.2	Competitive
L-threonine	7.3 ± 1.7	5.2 ± 0.2	0.7 ± 0.1	2.2 ± 0.4	Competitive

Assays were carried out in 100 μL of 100 mM Tris/HCl buffer (pH 9.0) containing 2 mM dithiothreitol, 1 mM EDTA, and 50 μM PLP, and 1–2 μg of the recombinant enzymes, at 37 °C for 20 min. The amount of α-keto acids generated was quantitated as described previously [14]. The L-serine and L-threonine concentrations ranging 1–64 mM were used to determine of kinetic parameters. To determine the K_i value for L-serine or L-threonine, the constant concentration (40 mM) of L-threonine or L-serine was used. All values are expressed as a mean ± S.E. of triplicates.

Table 2
Inhibition of recombinant EhTD1 by keto-acids.

	%Inhibition	
	Without AMP	With 5 mM AMP
Pyruvate	45.3 ± 1.7	44.6 ± 0.2
Glyoxylate	54.1 ± 1.2	49.6 ± 2.7
2-Oxobutyrate	49.3 ± 1.1	43.2 ± 3.8

TD activity was measured spectrophotometrically at 310 nm as described previously [15]. Effects of 20 mM of various keto acids (pyruvate, 2-oxobutyrate or glyoxylate) on the activity of rEhTD1 in the presence or absence of AMP (5 mM). TD activity is shown in percentage relative to that of TD activity measured in the absence of both keto acid and AMP. All values are expressed as a mean ± S.E. of triplicates.

(Table 1). Therefore, L-cysteine likely plays a role in the regulation of EhTD1, particularly serine dehydratase activity of EhTD1 at physiological concentrations. We also studied the effect of ATP, ADP, AMP, and CMP on the activity of rEhTD1. All of these nucleotides have been shown to be allosteric regulators of catabolic TDs from various sources [4]. rEhTD1 was inhibited by ATP in a dose-dependent manner (data not shown). It showed approximately 50% inhibition by 10 mM of ATP. In contrast to the catabolic TDs from bacteria plants and animals [4,15], rEhTD1 was insensitive to the allosteric activation by ADP, AMP, and CMP (data not shown). The AMP/CMP binding site of EhTD1 has three substitutions of Arg-53 to Lys-69, Asp-119 to Gly-135, and Gln-275 to Glu-291 (Fig. 2, "D"). The guanidium group of Arg-53 forms a hydrogen bond with the phosphate group of AMP or CMP. The side-chain oxygen atom of Asp-119 is hydrogen bonded to the N4 atom of the adenine moiety of AMP or the N3 atom of the cytosine moiety of CMP, whereas the side-chain oxygen atom of Gln-275 is involved in the hydrogen bonding with the N6 atom of the adenine moiety of AMP or the O2 atom of the cytosine moiety of CMP [4]. Absence of these hydrogen bonds might contribute to the lack of AMP or CMP binding to the enzyme. Allosteric activation by valine and inhibition by isoleucine were described for biosynthetic TDs [3]. However, in accordance with the catabolic nature, rEhTD1 was neither activated by valine nor inhibited by isoleucine (data not shown). We also investigated the effect of various catabolites on the activity of rEhTD1 in both the presence and absence of AMP. rEhTD1 was markedly inhibited by both the end products, i.e. pyruvate and 2-oxobutyrate, and also by glyoxylate (Table 2). Inhibition by these keto acids was not reversed by 5 mM AMP, which is dissimilar to the catabolic TD from various other sources. This is in accordance with the lack of allosteric activation of EhTD1 by AMP. Inhibition of catabolic TDs by the keto acids and reversal of the inhibition by AMP have been well documented [15]. Altogether, these findings indicate that the regulatory mechanisms of EhTD1 are distinct from that of bacterial, plant, and animal counterparts.

It has been shown that TD is developmentally regulated in *Dictyostelium discoideum* [19]. *D. discoideum* has both catabolic and biosynthetic TDs, and during the development of the vegetative to pseudoplasmodial stage, biosynthetic TD activity decreases while catabolic TD is upregulated [19]. Similarly, TD is also developmentally regulated in *Entamoeba*. Our transcriptome study showed that an *E. invadens* homologue of *EhTD1* gene is down regulated by 8 fold during the transition of trophozoites to the dormant cyst stage, suggesting its role in proliferation (Escueta et al., unpublished). In *Trypanosoma brucei*, which lacks TD, L-threonine is metabolized using the alternative aminoacetone pathway, which involves a mitochondrial threonine dehydrogenase and aminoacetone synthase. This route is not operational in *E. histolytica* and *Leishmania major* [20]. *L. major* has two pathways to metabolize L-threonine. L-threonine is converted to 2-oxobutyrate by TD, and then oxidized to succinyl CoA. Alternatively, L-threonine can be converted to L-glycine by serine hydroxymethyltransferase (SHMT). The resulting L-glycine can be converted to pyruvate via L-serine by the action of SHMT and TD. The later route of threonine catabolism does not operate in *Entamoeba* as a gene encoding SHMT is absent [7]. In *T. vaginalis*, which possesses TD, L-threonine and L-serine are also used for energy generation in the absence of carbohydrates [21]. In summary, we have characterized TD, one of the key enzymes that allow utilization of amino acids as energy source [22,23], from *E. histolytica*. Our findings should help to understand the significance of the amino acid catabolism for energy generation in *E. histolytica* [24].

Acknowledgements

We thank Kumiko Nakada-Tsukui, Fumika Mi-ichi, and all other members of our laboratory for the technical assistance and valuable discussions. This work was supported by a Grant-in-Aid for Scientific Research from the Ministry of Education, Culture, Sports, Science and Technology of Japan to T.N. (18GS0314, 18050006, 18073001), a grant for research on emerging and re-emerging infectious diseases from the Ministry of Health, Labour and Welfare of Japan (H20-Shinkosaiko-016), and a grant for research to promote the development of anti-AIDS pharmaceuticals from the Japan Health Sciences Foundation to T.N.

References

[1] Umbarger HE. Threonine deaminases. Adv Enzymol 1973;37:349–95.
[2] Phillips AT, Wood WA. The mechanism of action of 5′-adenylic acid-activated threonine dehydratase. J Biol Chem 1965;240:4703–9.
[3] Umbarger HE. Evidence for a negative feedback mechanism in the biosynthesis of isoleucine. Science 1956;123:848.
[4] Simanshu DK, Savithri HS, Murthy MRN. Crystal structures of *Salmonella typhimurium* biodegradative threonine deaminase and its complex with CMP provide structural insights into ligand-induced oligomerization and enzyme activation. J Biol Chem 2006;281:39630–41.
[5] World Health Organization/Pan American Health Organization Report. A consultation with experts on amebiasis. Epidemiological Bulletin/PAHO 1997;18:13–4.
[6] Müller M. Enzymes and compartmentation of core energy metabolism of anaerobic protists—a special case in eukaryotic evolution. In: Coombs GH, Vickerman K, Sleigh MA, Warren A, editors. Evolutionary Relationships Among Protozoa. Dordrecht, The Netherlands: Kluwer Academic Publishers; 1998. p. 109–32.
[7] Loftus B, Anderson I, Davies R, et al. The genome of the protist parasite *Entamoeba histolytica*. Nature 2005;433:865–8.
[8] Zuo X, Coombs GH. Amino acid consumption by the parasitic, amoeboid protists *Entamoeba histolytica* and *E. invadens*. FEMS Microbiol Lett 1995;130:253–8.
[9] Samarawickrema NA, Brown DM, Upcroft JA, Thammapalerd N, Upcroft P. Involvement of superoxide dismutase and pyruvate:ferredoxin oxidoreductase in mechanisms of Metronidazole resistance in *Entamoeba histolytica*. J Antimicrobial Chemother 1997;40:833–40.
[10] Reeves RE, Warren LG, Susskind B, Lo HS. An energy-conserving pyruvate-to-acetate pathway in *Entamoeba histolytica*. Pyruvate synthase and a new acetate thiokinase. J Biol Chem 1977;252:726–31.
[11] Takeuchi T, Weinbatch EC, Gottlieb M, Diamond LS. Mechanism of L-serine oxidation in *Entamoeba histolytica*. Comp Biochem Physiol B 1979;62:281–5.
[12] Diamond LS, Harlow DR, Cunnick CC. A new medium for the axenic cultivation of *Entamoeba histolytica* and other *Entamoeba*. Trans R Soc Trop Med Hyg 1978;72:431–2.
[13] Nozaki T, Asai T, Kobayashi S, et al. Molecular cloning and characterization of the genes encoding two isoforms of cysteine synthase in the enteric protozoan parasite, *Entamoeba histolytica*. Mol Biochem Parasitol 1998;97:33–44.
[14] Soda K. Microdetermination of D-amino acids and D-amino acid oxidase activity with 3-methyl-2-benzothiazolone hydrazone hydrochloride. Anal Biochem 1968;25:228–35.
[15] Shizuta Y, Kurosawa A, Inoue K, Tanabe T, Hayaishi O. Regulation of biodegradative threonine deaminase. I. Allosteric inhibition of the enzyme by a reaction product and its reversal by adenosin 5′-monophosphate. J Biol Chem 1973;248(2):512–20.
[16] Saito N, Robert M, Kochi H, et al. Metabolite profiling reveals YihU as a novel hydroxybutyrate dehydrogenase for alternative succinic semialdehyde metabolism in *Escherichia coli*. J Biol Chem 2009;284:16442–51.
[17] Bakker Grunwald T, Martin JB, Klein G. Characterization of glycogen and amino acid pool of *Entamoeba histolytica* by 13C-NMR spectroscopy. J Eukaryot Microbiol 1995;42:346–9.

[18] Leoncini R, Pagani R, Marinello E, Keleti T. Double inhibition of L-threonine dehydratase by aminothiols. Biochim Biophys Acta 1989;994:52–8.
[19] Pong SS, Loomis Jr WF. Replacement of an anabolic threonine deaminase by a catabolic threonine deaminase during development of *Dictyostelium discoideum*. J Biol Chem 1973;248:4867–73.
[20] Opperdoes F, Coombs GH. Metabolism of *Leishmania*; proven and predicted. Trends Parasitol 2007;23:149–58.
[21] Zuo X, Lockwood BC, Coombs GH. Uptake of amino acids by the parasitic, flagellated protist *Trichomonas vaginalis*. Microbiology 1995;141:2637–42.
[22] Tokoro M, Asai T, Kobayashi S, Takeuchi T, Nozaki T. Identification and characterization of two isoenzymes of methionine γ-lyase from *Entamoeba histolytica*. J Biol Chem 2003;278:42717–27.
[23] Sato D, Yamagata W, Harada S, Nozaki T. Kinetic characterization of methionine γ-lyases from the enteric protozoan parasite *Entamoeba histolytica* against physiological substrates and trifluoromethionine, a promising lead compound against amoebiasis. FEBS J 2008;275:548–60.
[24] Nozaki T, Ali V, Tokoro M. Sulfur-containing amino acid metabolism in parasitic protozoa. Adv Parasitol 2005;60:1–99.

IUBMB *Life*, 61(11): 1019–1028, November 2009

Critical Review

Methionine Gamma-Lyase: The Unique Reaction Mechanism, Physiological Roles, and Therapeutic Applications Against Infectious Diseases and Cancers

Dan Sato[1,2] and Tomoyoshi Nozaki[3]

[1]*Institute for Advanced Biosciences, Keio University, Tsuruoka, Yamagata, Japan*

[2]*Center for Integrated Medical Research, School of Medicine, Keio University, Shinjuku, Tokyo, Japan*

[3]*Department of Parasitology, National Institute of Infectious Diseases, Shinjuku, Tokyo, Japan*

Summary

Sulfur-containing amino acids (SAAs) are essential components in many biological processes and ubiquitously distributed to all organisms. Both biosynthetic and catabolic pathways of SAAs are heterogeneous among organisms and between developmental stages, and regulated by the environmental changes. Limited lineage of organisms ranging from archaea to plants, but not human, possess a unique enzyme methionine gamma-lyase (MGL, EC 4.4.1.11) to directly degrade SAA to α-keto acids, ammonia, and volatile thiols. The reaction mechanisms and the physiological roles of this enzyme are partially demonstrated by the enzymological analyzes, structure determination, isotopic labeling of the intermediate metabolites, and functional analyzes of deficient mutants. MGL has been exploited as a drug target for the infectious diseases caused by parasitic protozoa and anaerobic periodontal bacteria. In addition, MGL has been utilized to develop therapeutic interventions of various cancers, by introducing recombinant proteins to deplete methionine essential for the growth of cancer cells. In this review, we discuss the current understanding of enzymological properties, putative physiological roles, and therapeutic applications of MGL. © 2009 IUBMB

IUBMB *Life*, 61(11): 1019–1028, 2009

Keywords sulfur-containing amino acid; pyridoxal 5′-phosphate; protozoa; periodontal bacteria; cancer.

Abbreviations MGL, methionine gamma-lyase; SAA, sulfur-containing amino acid.

Received 19 June 2009; accepted 5 August 2009

Address correspondence to: Tomoyoshi Nozaki, Department of Parasitology, National Institute of Infectious Diseases, 1-23-1 Toyama, Shinjuku, Tokyo 162-8640, Japan. Tel: +81-3-5285-1111 ext. 2600. Fax: +81-3-5285-1219. E-mail: nozaki@nih.go.jp

ISSN 1521-6543 print/ISSN 1521-6551 online
DOI: 10.1002/iub.255

INTRODUCTION

Sulfur is an essential element in all living organisms. Bacteria and plants incorporate sulfur as inorganic compounds such as sulfate, sulfite, and sulfide. In contrast, most of heterotrophs take in sulfur as sulfur-containing amino acids (SAAs) synthesized by other organisms. SAAs play critical roles in a variety of biological processes including protein synthesis, methylation, biosynthesis of vitamins, polyamines, and antioxidants. SAAs are ubiquitously distributed, but their metabolic pathways diverged among organisms, and are modulated in the life cycle and upon stresses and changes in environmental conditions (*1*).

Both biosynthesis and degradation of SAAs (a simplified scheme is shown in Fig. 1) must be tightly regulated. The maintenance of low homocysteine concentrations is essential not only for a proper flow of sulfur in the transsulfuration pathway and the methionine cycle, but also for evading toxic effects of the molecule, which has been implicated in pathological conditions associated with various genetic disorders causing homocystinuria and homocysteinemia (*2*). Homocysteine has also been shown to be the pro-oxidant causing damage to the vascular endothelia (*3*), and associated with an increased cardiovascular risk (*4*) and Alzheimer's disease (*5*).

In mammals, SAAs are mainly degraded via oxidative cysteine catabolism, where cysteine dioxygenase (EC. 1. 13. 11. 20) catalyzes the oxygenation of cysteine to 3-sulfinoalanine, a key intermediate of cysteine metabolism leading to hypotaurine, taurine, pyruvate, and sulfate (*6*). The other cysteine degradative pathway in mammals is initiated by cysteine aminotransferase (EC. 2. 6. 1. 3), which deaminates cysteine to form 3-mercaptopyruvate. The SAA biosynthesis and degradation in mammals have recently been reviewed by Stipanuk (*2*). In the organisms that possess a methionine biosynthetic pathway, such as bacteria and plants, cystine (a pair of cysteines joined by a disulfide bond) is also degraded at least *in vitro* by cystathionine beta-lyase (EC. 4. 4. 1. 8) to thiocysteine, pyruvate, and ammonia

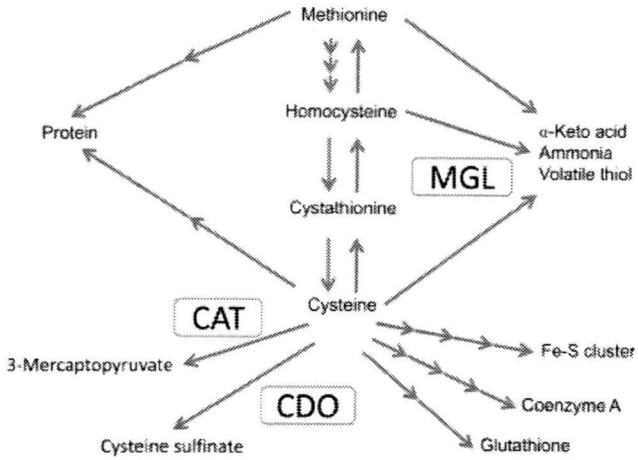

Figure 1. A general scheme of transsulfuration, methionine cycle, and sulfur-containing amino acid degradation. The enzymes involved in sulfur-containing amino acid degradation are boxed. MGL, methionine gamma-lyase; CDO, cysteine dioxygenase; CAT, cysteine aminotransferase. [Color figure can be viewed in the online issue, which is available at www.interscience.wiley.com.]

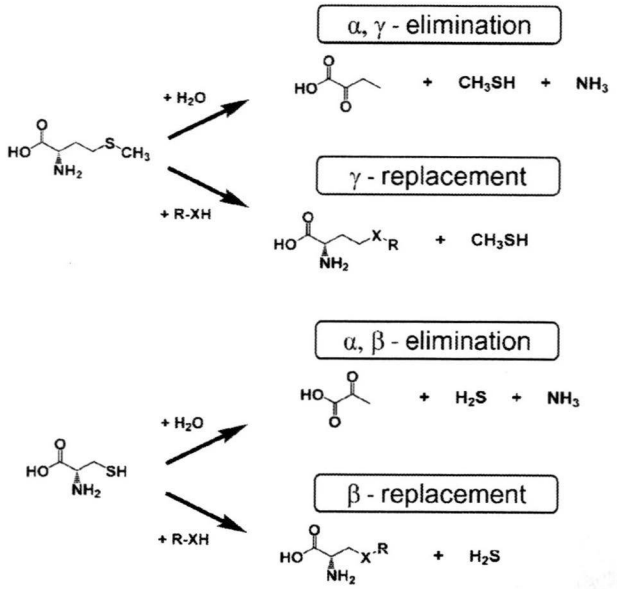

Figure 2. Catalytic reactions of MGL. α, γ-elimination and γ-replacement of L-methionine (upper) and, the α, β-elimination and β-replacement of L-cysteine (lower) are indicated. X=S or Se.

(*7, 8*). On the other hand, a limited lineage of organisms possess the unique pathway, in which SAAs are converted to α-keto acids, ammonia, and volatile thiols by methionine gamma-lyase (MGL, EC. 4. 4. 1. 11).

Since Onitake reported 70 years ago that some bacteria produced methanethiol (*9*), MGL has been characterized from bacteria, including *Clostridiums porogenes* (*10*), *Pseudomonas ovalis* (*11*), *Pseudomonas putida* (*12*), *Aeromonas* sp. (*13*), *Citrobacter intermedius* (*14*), *Brevibacterium linens* (*15*), *Citrobacter freundii* (*16*), *Porphyromonas gingivalis* (*17*), and *Treponema denticola* (*18*), parasitic protozoa such as *Trichomonas vaginalis* (*19*), *Entamoeba histolytica* (*20*), and a model plant *Arabidopsis thaliana* (*21*). MGL activity was also detected from archaeon *Ferroplasma acidarmanus* (*22*), cheese surface bacteria such as *Micrococcus luteus, Arthrobacter* sp., *Corynebacterium glutamicum,* and *Staphylococcus equorum* (*23*). Crystal structures have been reported from *Pseudomonas putida,* (*24-26*), *Citrobacter freundii* (*27, 28*), *Trichomonas vaginalis* (PDB ID: 1E5F and 1PFF), and *Entamoeba histolytica* (*29, 30*). In this review, we outline our current understanding of the distribution among organisms, enzymological properties, and the reaction mechanisms of MGL. We then discuss the present status of practical applications exploiting MGL, namely drug development against pathogens and cancers.

ENZYMOLOGICAL PROPERTIES

Basic Reactions, Size, and Cofactor

MGL catalyzes the α, γ-elimination of L-methionine and its derivatives such as L-homocysteine, L-ethionine, and L-selenomethionine (Fig. 2). It also catalyzes the α, β-elimination of L-cysteine and its analogs such as *S*-methyl-L-cysteine (*31*). These reactions yield α-keto acid (2-oxobutyrate and pyruvate), ammonia, and thiols (methanethiol and hydrogen sulfide). It also degrades *O*-substituted serine or homoserine such as *O*-acetyl-L-serine, *O*-acetyl-L-homoserine, and *O*-succinyl-L-homoserine, and release organic acids instead of thiols. This enzyme alternatively catalyzes β- or γ-replacement reactions, where the sulfur or oxygen atom at the β- or γ-position of the substrate is replaced with the thiol. For example, the methy thiol moiety of L-methionine is replaced by ethanethiol to yield ethionine and mechanethiol (*11*). MGL also catalyzes deamination and γ-addition reaction of L-vinylglycine (*31*). MGL consists of 389–441 amino acids, and forms homotetramer. The active MGL tetramer consists of two sets of the catalytic dimers (Fig. 3, panel A; green/yellow and red/blue pairs) that are tightly associated. (*24, 26, 27*). The active site is formed at the interface of the two neighboring subunits. Each subunit contains one pyridoxal 5′- phosphate (PLP) as a cofactor (Fig. 3, panel B). MGL is categorized into the γ-family of PLP-dependent enzymes (*32*).

Reaction Mechanisms

Based on the reaction mechanism of PLP γ-family enzymes hitherto known and the enzymological analyzes of *P. putida* MGL wild-type and mutants, it has been proposed that MGL catalyzes elimination reaction in the following order: (1) a Schiff-base linkage between PLP and the lysine residue displaces the binding of the primary amino group of the substrate and

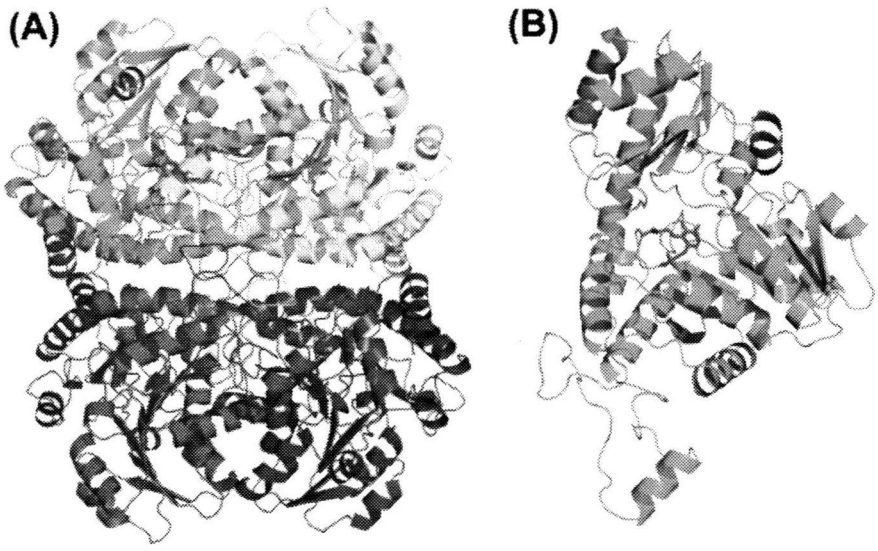

Figure 3. Crystal structure of MGL. (A) The overall structure of *E. histolytica* MGL2. (Harada et al., unpublished). Each subunit consisting the homotetramer is indicated in green, yellow, red, and blue. PLP is indicated in magenta. (B) A single subunit of *E. histolytica* MGL2.

PLP, to form an external aldimine, (2) α- and β-hydrogens of the substrate are shifted to PLP, (3) the phenolic group of the adjacent tyrosine residue attacks the γ-position of the substrate as an acid catalyst, (4) the thiol group is eliminated from the substrate, and (5) α-keto acid and ammonia are released from PLP (*31, 33, 34*) (Fig. 4). The mutational studies of *E. histolytica* MGL supported the assumption of an acid catalyst of the tyrosine residue (*35*).

Amino Acid Residues Implicated in Catalysis

Recently, structural analysis of *P. putida* MGL revealed that the six amino acid residues, Tyr59, Arg61, Tyr114, Cys116, Lys240, and Asp241 are located in the vicinity of the substrate binding pocket, close to PLP (*26*). Aside from the amino acid residues conserved among PLP γ-family enzymes (*20, 24-26, 36*), a line of evidence indicates that Cys116 of *P. putida* MGL takes part in the unique enzymatic reactions of MGL. This cysteine is not conserved in other PLP γ-family enzymes, and substituted by glycine or proline in cystathionine γ-lyase, cystathionine β-lyase, and cystathionine β-synthase (*26*), and thus was previously suggested to be involved in the recognition and γ-elimination of methionine (*37*). Unlike other MGLs, *B. linens* MGL degrades neither cysteine nor cystathionine, whereas *A. thaliana* MGL degrades cysteine, but hardly cystathionine (*38*). In both *B. linens* and *A. thaliana* MGL, the corresponding cysteine residue was substituted by glycine (*15, 38*).

The mutational studies of *E. histolytica* and *T. vaginalis* MGL isozymes also demonstrated that the corresponding cysteine residue directly contributes to the substrate specificity. When this cysteine was replaced with glycine or serine, the Km values of one isozyme for methionine and cysteine were drastically changed, while those of the other isotype remained unaltered (*35, 39*).

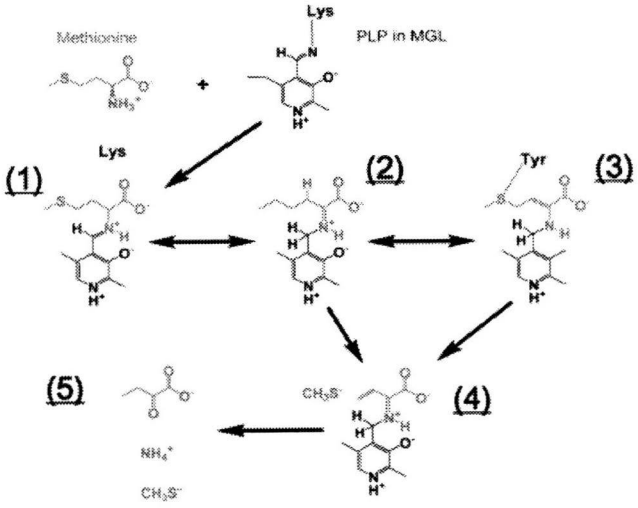

Figure 4. A proposed reaction process of α,γ-elimination of methionine by MGL [modified from (*31, 33, 34*)]. Substrates, intermediates, and products are shown in red, while PLP is shown in black. Structures (*1*) to (*5*) correspond to the reaction intermediates explained in the text.

In *P. putida* MGL, chemical modification with 2-nitrothiocyanobenzoic acid and labeling with a PLP analog, N-(bromoacetyl)pyridoxamine phosphate, suggested the catalytic importance of Cys116 (*40, 41*). The substitution of this cysteine to

Table 1
Summary of the fates and roles of the degradation products generated by MGL in various organisms

Products	Final products	Physiological roles	Organisms	Reference
2-Oxobutyrate	Propionate	ATP generation[a]	Anaerobic bacteria	42
			Parasitic protozoa	43 (See Fig. 5)
	Isoleucine	Isoleucine biosynthesis[b]	Plant (*A. thaliana*)	21
	2,3-pentanedione	Unknown	Cheese ripening bacteria	44
Methanethiol	Methanethiol	Host invasion[b] (pathogenicity)	Periodontal bacteria	17
	Methanethiol Dimethyl disulfide Dimethyl trisulfide Thioesters	Unknown (Odor formation of cheese)	Cheese ripening bacteria	44, 45
	S-methyl-cysteine	Sulfur storage[a]	Plant (*A. thaliana*)	21
	Methanethiol Dimethyl sulfide Dimethyl disulfide Dimethyl trisulfide	Defense against herbivorous insects[c]	Plant (guava)	46

[a]Roles only suggested.
[b]Roles experimentally demonstrated.
[c]The presence of *MGL* gene is confirmed only in *A. thaliana*, but not in guava. The volatile thiols may be produce by enzymes other than MGL in guava leaves.

histidine caused a drastic increase or decrease in the activity of MGL toward cysteine or methionine, respectively; their catalytic efficiency (kcat/Km) for cysteine increased by 16.2 fold, while that for methionine decreased by 552 fold, mainly due to the reduction in kcat (*37*). Similar changes in the activity were also observed for methionine and cysteine analogs (*37*).

The crystal structure revealed that the cysteine residue is located in the proximity of a tyrosine residue (*24*), which attacks the γ-position of the substrate (*33*) [see Fig. 4, intermediate (*3*)]. However, direct interaction between the cysteine residue of MGL and methionine, as a substrate, was not observed. Thus, the structures of MGL/methionine intermediates at various reaction stages should be resolved to elucidate how the cysteine residue is involved in γ-elimination of methionine.

PHYSIOLOGICAL FUNCTIONS

The physiological roles of MGL have been either directly demonstrated or indirectly suggested in several organisms (summarized in Table 1).

Association with Anaerobic Metabolism

Anaerobic bacteria and parasitic protozoa that possess MGL, rely on glycolysis and amino acid degradation for energy generation (*42*, *46*). In those anaerobic organisms, for example, anaerobic amitochondrial parasites, pyruvate is converted to acetate via acetyl-CoA (Fig. 5). The conversion proceeds in two sequential reactions catalyzed by pyruvate:ferredoxin oxidoreductase (PFOR, EC. 1. 2. 7. 1) and acetate-CoA ligase (ADP-forming) (EC. 6. 2. 1. 13). In this process, one ATP is generated from one pyruvate. As 2-oxobutyrate, generated from

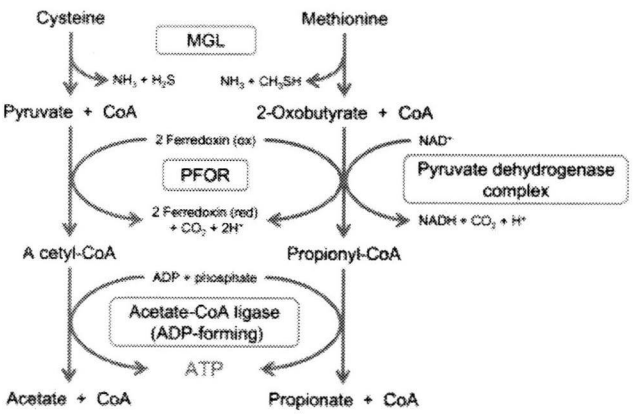

Figure 5. A proposed reaction scheme of energy generation from 2-oxobutyrate. 2-Oxobutyrate, generated from methionine by MGL, serves as a substrate for PFOR or pyruvate dehydrogenase complex, which leads to the ATP generation. "ox" and "red" are the oxidized and reduced form of ferredoxin, respectively. [Color figure can be viewed in the online issue, which is available at www.interscience.wiley.com.]

methionine by MGL, is condensed with CoA to form propionyl-CoA, which is in turn decomposed by acetate-CoA ligase (ADP-forming) with a concomitant ATP generation, the process might contribute to energy metabolism.

The Bioenergetic Roles of MGL in Bacteria

In *P. putida*, MGL gene is transcribed as a part of an operon containing 2-oxobutyrate decarboxylase (*47*, *48*), both of which

appear to be coordinately regulated (Inoue and Inagaki, unpublished). Although 2-oxobutyrate decarboxylase is homologous to homodimeric-type E1 component of pyruvate dehydrogenase complex (*47, 48*), its catalytic efficiency (kcat/Km) is 29-fold higher for 2-oxobutyrate than toward pyruvate (*47, 48*). E2 component, which produces acetyl-CoA by transferring the acetyl group to CoA, is also annotated in the genome database (http://www.pseudomonas.com/). Although E3 (dihydrolipoyl dehydrogenase) appears to be absent in the genome, it is conceivable that *P. putida* is capable of producing ATP via this pathway.

The Other Roles of MGL in Bacteria

MGL has been implicated in the pathogenicity of periodontal bacterium, *P. gingivalis* using a mouse model (*17*). It was shown that only 7.7% of mice infected with wild-type *P. gingivalis* survived, whereas 36% of mice infected with MGL-deficient mutant survived, at 4 days after subcutaneous injection of bacteria. No direct evidence for the involvement of MGL in the pathogenesis in other bacteria is available.

In the cheese ripening bacterium *B. linens*, methanethiol and 2-oxobutyrate are produced by MGL (*44*). Methanethiol is converted to dimethyl disulfide, dimethyl trisulfide, and thioesters, and 2-oxobutyrate is condensed with active acetaldehyde derived from pyruvate, and metabolized to 2,3-pentanedione (acetyl propionyl) (*44*). This condensation reaction is catalyzed by acetolactate synthase (*44, 45*). Under the methionine-rich conditions, genes encoding MGL, acetolactate synthase (see below), and α-keto acid dehydrogenases are up-regulated (*45*). Thus, methionine degradation is tightly linked with carbohydrate metabolism in this and related bacteria. The physiological importance of 2,3-pentanedione has not been demonstrated.

The Roles of MGL in Plants

In the model plant *A. thaliana*, MGL is expressed in various tissues. The regulation of its expression in seeds is peculiar. It was shown that while MGL mRNA was highly accumulated but not translated in dry seeds, the protein was highly expressed in imbibed seeds (*21*). This unique regulation of MGL expression suggests that immediate production of MGL protein is essential in the early germination process. These data suggest that while MGL is implicated in methionine homeostasis in various tissues, it plays an important role in the resumption process (*21*).

Methanethiol and 2-oxobutyrate, the degradation products of methionine by MGL, are used for the synthesis of *S*-methyl-L-cysteine and isoleucine, respectively. *S*-methyl-L-cysteine is a potential storage molecule of sulfur, similar to the metabolites of methionine cycle such as *S*-adenosyl-L-methionine, and *S*-methyl-L-methionine (*21*). Functional analysis of a MGL-deficient *A. thaliana* mutant revealed that MGL is involved in the alternative reverse-transsulfuration pathway, in which methionine is metabolized to cysteine, not via cystathionine (*38*). Methanethiol was potentially an intermediate of this pathway, although a detailed process of flux was elusive (*38*). However, the methionine degradation by *A. thaliana* MGL was three orders of magnitude lower than that by MGL from other organisms, for example, the kcat/Km values of *A. thaliana* MGL was 0.0022 S^{-1} mM^{-1}, whereas those of *P. putida* and *E. histolytica* were 54 and 2.99, respectively (*33, 35, 38*). Therefore, the possibility that *A. thaliana* MGL predominantly catalyzes a replacement reaction, rather than degradation, was not excluded. More detailed enzymological characterization including identification of an acceptor of methanethiol is necessary to fully characterize the pathway.

Recently, it has been reported that wounded leaves of guava produce the volatile sulfur compounds including methanethiol as defense molecules against herbivorous insects (*46*). Although MGL has not yet been demonstrated in guava, and it remains unknown if this mechanism exists ubiquitously in plants, the productions of sulfur compounds with anti-insect activity might be the major physiological function of MGL in plants.

Function and Lateral Gene Transfer-Dependent Acquisition of MGL Isotypes in Parasitic Protozoa

Both of the MGL-containing parasitic protists *E. histolytica* and *T. vaginalis* possess two isozymes of MGL with high mutual identity (69%) and distinct substrate specificities (*20, 35, 39*). In *E. histolytica*, one isozyme (i.e., *Eh*MGL1) degrades methionine more efficiently than homocysteine, while the other (*Eh*MGL2) prefers homocysteine to methionine (*35, 39*). In contrast, one isozyme of *T. vaginalis* MGL (*Tv*MGL1) seems predominantly to degrades methionine, homocysteine, and cysteine compared to the other (*Tv*MGL2) (*35, 39*). Considering that MGL isozymes have been found only in the parasitic protozoa, the multiplicity of MGLs might be related to the parasitic style or pathogenesis.

It was proposed that MGL in extant protozoan parasites was acquired by lateral gene transfer, together with the enzymes related to anaerobic energy metabolism (*20, 49*). Interestingly, the origin of MGL in the two parasitic protozoa was not identical (*20*). *E. histolytica* MGLs show a monophylic relationship with MGL from archaea, while *T. vaginalis* MGLs have strong affinity to MGLs of bacterial origin, suggesting that lateral gene transfer of MGL to the two protists occurred independently.

Other Undiscovered Roles

Since the substrate specificity of MGL varies among organisms, the physiological role of MGL, other than the maintenance of SAA homeostasis, can be also organism specific. Although MGL catalyzes homocysteine *in vitro*, it remains questionable whether it is responsible for the degradation of homocysteine *in vivo* because the cellular concentrations of homocysteine are predicted to be extremely low [e.g., the concentration in human plasma is less than 10 μM (*50*)] compared to the Km values of MGLs.

The physiological role of MGL has not been investigated in archaea. In an acidophilic iron-oxidizing euryarchaeon